ABSTRACT

Title of Thesis: ADAPTIVE LOG DOMAIN FILTERS USING FLOATING GATE TRANSISTORS

Yiming Zhai, Master of Science, 2004

Thesis Directed By: Professor Pamela A. Abshire
Department of Electrical and Computer Engineering

In this thesis, an adaptive first order lowpass log domain filter and an adaptive second order log domain filter are presented with integrated learning rules for model reference estimation. Both systems are implemented using multiple input floating gate transistors to realize on-line learning of system parameters. Adaptive dynamical system theory is used to derive robust control laws in a system identification task for the parameters of both a first order lowpass filter and a second order tunable filter. The log domain filters adapt to estimate the parameters of the reference filters accurately and efficiently as the parameters are changed. Simulation results for both the first order and the second order adaptive filters are presented which demonstrate that adaptation occurs within milliseconds. Experimental results and mismatch analysis are described for the first order lowpass filter which demonstrates the success of our adaptive system design using this model-based learning method.

ADAPTIVE LOG DOMAIN FILTERS USING FLOATING GATE TRANSISTERS

By

Yiming Zhai

Thesis submitted to the Faculty of the Graduate School of the
University of Maryland, College Park, in partial fulfillment
of the requirements for the degree of
Master of Science
2004

Advisory Committee:
Professor Pamela A. Abshire, Chair/Advisor
Professor Robert W. Newcomb
Professor Martin C. Peckerar

Dedication

To my parents.

Acknowledgements

I would like to acknowledge people who have contributed to this project and helped me during the two and a half years' study and research.

The first person I want to thank is my advisor, Professor Pamela A. Abshire. I want to thank her not only because of her broad knowledge and her profound insights, but also because of her decent, warm, sensitive and caring personality. She gave me a promising and significant research project, and strong encouragement and full support. I would like to thank her for her trust and confidence in me and her appreciation of my work.

I wish to thank Dr. Marc H. Cohen who gave me a lot of help on my research work. He has spent an enormous amount of time to help me to solve the testing problems and work on the circuits. I wish to thank Yanyi L. Wong who was a research partner in the previous part of the project and taught me a lot about the use of HSPICE simulator and MAGIC layout tool.

I wish to thank Honghao Ji, Peng Xu, Makeswaran Loganathan, Suvarcha Malhotra, Somashekar B. Prakash, Nicole M. Nelson, Alfred M. Haas and Shalom Rosenfeld for their kind assistance and useful discussions.

I wish to thank Professor Robert W. Newcomb and Professor Martin C. Peckerar for serving on my thesis exam committee.

I also thank Laboratory for Physics Sciences for supporting the project and MOSIS service for providing chip fabrication.

Finally, I give my greatest thanks to my parents for their unconditional support and love.

Table of Contents

Dedication ii
Acknowledgements iii
Table of Contents iv
List of Figures v
Chapter 1: Introduction 1
1.1 Background and Motivation 1
1.2 Multiple Input Translinear Element 3
1.3 Organization of the thesis 5
1.4 Contributions 6
Chapter 2: Adaptation of First Order Lowpass Filters 7
2.1 Derivation of Learning Rules 7
2.2 Circuit Implementation 12
2.2.1 MITE Implementation of Log Domain First Order Lowpass filters 12
2.2.2 MITE Implementation of Learning Rules 14
2.3 Simulation Results 20
2.4 Experimental Results 23
2.5 Analysis of Current Mirror Ratio Mismatch and Compensation 30
2.6 Summary 40
Chapter 3: Adaptation of Second Order Filters 41
3.1 Second Order Filter Design 41
3.1.1 First Order Lowpass filter structure 43
3.1.2 Second Order Bandpass Filter structure 44
3.1.3 Simulation Results 50
3.2 Derivation of Learning Rules 54
3.3 Circuit Implementation 59
3.3.1 Implementation of Log Domain Second Order Filters 59
3.3.2 Implementation of Learning Rules 62
3.4 Simulation Results 66
3.5 Summary 69
Chapter 4: Conclusions and Future work 70
Bibliography 72

List of Figures

Figure 1.1: Circuit symbol for ideal N-input MITE. 4
Figure 2.1: The system identification problem: an input *u* is applied to both plant and model filters. The error e_1 is the difference of plant and model outputs $(x_2 - x_1)$ and is used to adapt the parameters of the model $(\overline{A}, \overline{B})$. 8
Figure 2.2: (a) Log domain MITE filter for a first order lowpass transfer function used as the unknown plant; (b) Log domain MITE implementation for adaptive model. 13
Figure 2.3: Circuit for computing temporal derivative with mismatch controllers. 16
Figure 2.4: Circuit for four quadrant multiplication. 18
Figure 2.5: MITE implementation of learning rules for gain and time constant. 19
Figure 2.6: Technique used to avoid floating-node problems in the simulator. 21
Figure 2.7: Adapting with a 10kHz square wave input. 21
Figure 2.8: Adapting with 4 harmonic sine waves. 22
Figure 2.9: Adapting with 14 geometrically spaced sine waves from 5-97kHz. 22
Figure 2.10: Testing setup for the adaptive first order lowpass filters including schematics of input voltage-current converter Howland current source, on-chip current conveyors, and output current-voltage converters. 25
Figure 2.11: Testing results of adaptation process: (a) error of outputs of plant and model filters. (b) gain control voltages of plant and model filters. (c) time constant control voltages of plant and model filters..... 27
Figure 2.12: Testing results of adaptation process: changes of gain voltages and time constant voltages to demonstrate condition 2 in mismatch analysis..... 28
Figure 2.13: Testing results of adaptation process: changes of gain voltages and time constant voltages to demonstrate condition 3 in mismatch analysis..... 29
Figure 3.1: MITE implementation for first order lowpass filter 42
Figure 3.2: Circuit for implementing Equation (3.12): (a) a straightforward idea which is unrealizable; (b) equivalent implementation..... 46
Figure 3.3: Circuit for implementing Equation (3.13): (a) a straightforward idea which is unrealizable; (b) equivalent implementation..... 46

Figure 3.4: Circuit for second order filter with dependent current sources. 48
Figure 3.5: Complete circuit for the second order filter. 48
Figure 3.6: Complete circuit for the second order bandpass filter..... 49
Figure 3.7: Time constant τ tuning with time constant current swept from 20nA to 60nA linearly with V_r=V_{gain}=0.75V and V_Q=1.45V 52
Figure 3.8: Quality factor Q tuning with voltage V_Q swept from 1.43V to 1.47V linearly with V_r=V_{gain}=0.75V and I_B=40nA..... 52
Figure 3.9: Gain dependence on gain control voltage V_g with I_B=40nA and V_Q=1.45V.. 53
Figure 3.10: The system identification problem. 55
Figure 3.11: (a) Log domain MITE network for a second order filter used for plant; (b) Log domain MITE implementation for filter. 61
Figure 3.12: (a) and (b) are circuits for computing temporal derivative of voltage; (c) is the circuit for computing temporal derivative of the current output difference. 64
Figure 3.13: (a) Circuit for computing four quadrant multiplication for quality factor adaptation; (b) Integrator circuit for quality factor adaptation; (c) Circuit for computing four quadrant multiplication for time constant adaptation; (d) Integrator circuit for time constant adaptation. 65
Figure 3.14 Technique used to avoid floating-node problems in the simulator. 67
Figure 3.15: 10kHz sine wave input signal: (a) Quality factor adaptation. (b) Time constant adaptation. (c) Output error. 67
Figure 3.16: Four harmonic sine waves input signal: (a) Quality factor adaptation. (b) Time constant adaptation. (c) Output error. 68
Figure 3.17: Six geometrically spaced sine waves from 10-96kHz input signal: (a) Quality factor adaptation. (b) Time constant adaptation. (c) Output error. ... 68

Chapter 1: Introduction

1.1 Background and Motivation

Adaptive signal conditioning is an important and well-established tool used widely in scientific and engineering disciplines such as communications, biomedical engineering and life science. Many complex and demanding applications require adaptive filtering to reject noise and improve signal performance dynamically. To achieve this, control laws must use limited information to adjust parameters of the adaptive system in directions that produce robust system adaptation. In this thesis, current-mode log domain filter architecture and floating gate MOSFETs are combined to realize accurate and stable learning rules for the system parameters of a first order lowpass filter and a second order bandpass filter.

Several groups have described filtering applications based on floating gate MOS circuits. Hasler et al. [1] described the Auto-zeroing Floating Gate Amplifier (AFGA) and its use in bandpass filter structures with very low frequency response capability. Fernandez et al. [2] described a 1V micropower lowpass filter implemented using Floating Gate Metal Oxide Semiconductor (FGMOS) transistors. Rodriguez-Villegas et al. [3] designed a log domain integrator based on FGMOS transistors. Minch [4, 5, 6] developed circuits and synthesis techniques using Multiple Input Translinear Elements (MITEs) for a variety of signal processing applications.

Other groups have reported current-mode filter implementations using transistors working in strong inversion mode. El-Masry and Gates [7] described a continuous-time

current-mode differentiator constructed using a capacitively coupled current mirror, which is simple, small in size and easily used in implementing higher order filters. Wu and El-Masry [8] described current-mode ladder filters using output current conveyors based on the simulation of the passive RLC ladder prototypes. The designs show that the multiple output current conveyor based circuits can reduce the number of active components by 50%. In contrast, we describe current-mode log domain filters using transistors working in weak inversion mode. Weak inversion mode is especially suitable for low power circuit design. The current flowing in a unit transistor working in weak inversion is below hundreds of nanoamperes, which is smaller than the values associated with strong inversion operation. The gate to source voltage drop of a transistor working in weak inversion is around or below the threshold voltage, which makes it possible to use low supply voltages and further reduce power consumption. In addition to the low power dissipation, the exponential transfer function in weak inversion also provides an extended dynamic range and easy tunability.

Few groups have reported integrated analog adaptive filters. Juan et al. [9] and Stanacevic and Cauwenberghs [10] have designed analog transversal Finite Impulse Response (FIR) filters that include adaptation of weights. Ferrara and Widrow [11] have designed a time-sequenced adaptive filter. The filter is an extension of the LMS adaptive filters which allow the weight vector to change freely in time in order to accommodate rapid changes in the statistics of a certain class of nonstationary signals, while allowing slow precise adaptation. All of these use Least Mean Square (LMS)-based adaptation algorithms. The output of the adaptive filter is defined by a weighted sum of input sequences. The Least Mean Square method is a steepest descent search algorithm which

adjusts weights iteratively in such a way as to move along the error surface towards the optimum value. The adaptive filters are digital filters composed of a tapped delay line and adjustable weights, whose impulse response is controlled by the adaptive algorithm. The individual weight values do not indicate any information or characteristics about the transfer function of the unknown system. The adaptation of the filter is input-dependent. Once the input signal varies, new values of weights are required to be calculated for adaptation. The method we present in this thesis is a model-based method. To estimate an unknown system, we first assume a transfer function model for it, and use another similar tunable structure as the estimator to track the operation of the unknown system. The output difference between the unknown system and the estimated system are used to derive adaptive laws of the variables which control the estimated system. The variables we select to adapt are parameters which control the characteristic of the filter transfer function. Once they are adapted using a certain input signal, the characteristic of the filter is determined. When the input signal changes, there is no further adaptation needed unless the transfer function of the unknown system changes. There is another point that LMS methods are well suited to implementations of FIR filters. In this thesis we present methods based on Lyapunov stability well suited for adaptive control of Infinite Impulse Response (IIR) filters. IIR filters offer the advantage of smaller filter structures and fewer filter coefficients than FIR filters in order to model plants of similar complexity.

1.2 Multiple Input Translinear Element

Multiple input translinear elements (MITEs) provide compact and elegant implementations of log domain filters. A MITE produces an output current that is an exponential function of the weighted sum of its input voltages. We can implement such

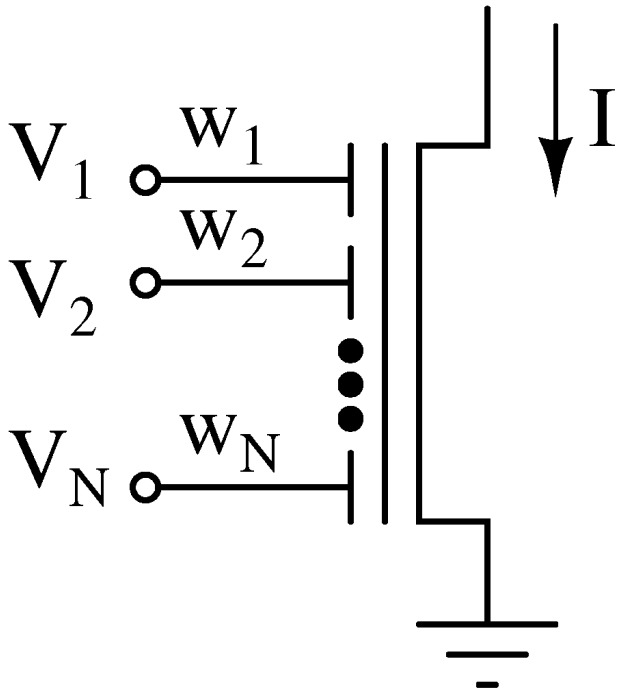

Figure 1.1: Circuit symbol for ideal N-input MITE.

devices using multiple input floating gate transistors operating in weak inversion. Figure 1.1 is a circuit symbol for an ideal N-input MITE. The transfer function of this element is given by:

$$I = I_0 \exp\left[\kappa(w_1 V_1 + w_2 V_2 + \cdots + w_N V_N)/U_T\right] \qquad (1.1)$$

where I_0 is a pre-exponential scaling current,

$$I_0 = \frac{2\mu C_{ox}\frac{W}{L}U_T^2}{\kappa} \qquad (1.2)$$

V_i is the ith input voltage, and w_i is the dimensionless positive weight of V_i. κ is the subthreshold slope factor which reflects the capacitive division between gate and substrate and is less than 1. U_T is the thermal voltage kT/q. The pre-exponential current I_0 depends on the carrier mobility μ, gate oxide capacitance C_{ox}, width to length ratio W/L, subtheshold slope factor κ and thermal voltage $U_T = kT/q$. The advantage of using floating gate MOS transistors in weak inversion to implement MITEs is that they can be easily fabricated in standard CMOS processes.

1.3 Organization of the thesis

Chapter 2 describes the adaptation of first order lowpass filters. The learning rules for robust adaptation for the first order lowpass filter are derived using the Lyapunov method. MITE implementations of the circuits are described and simulation results verify proper operation of the design. Experimental results demonstrate successful adaptation. We investigate the adaptive behavior under the non-ideal condition of a current mirror ratio mismatch. Chapter 3 describes the adaptation of second order bandpass filters. The design of a second order filter is presented. The Lyapunov method is used to investigate the

stability and derive the learning rules for the second order filters. Circuit implementations of the learning rules and simulation results with HSPICE using BSIM3v3 models for a 0.5μm technology are shown. Chapter 4 summarizes and draws conclusion from this work.

1.4 Contributions

My work in this project can be summarized as follows.

1. Fabricate through MOSIS and test the adaptive first order lowpass filters

2. Investigate the adaptive behavior under the non-ideal condition of a current mirror ratio mismatch.

3. Design and simulate a second order bandpass filter

4. Derive learning rules for adaptation of the second order filter topology

5. Design and simulate the adaptive second order filters

Chapter 2: Adaptation of First Order Lowpass Filters

Adaptive circuit designs [12] for log domain first order lowpass filters implemented by floating gate transistors are presented in this chapter. In section 2.1, learning rules for robust adaptation for the first order lowpass filter are derived. The Lyapunov method is used to investigate the stability of the adaptive system. In section 2.2, MITE implementations of the circuits are described. The log domain filter architecture is used to implement the filters. MITE circuits are used to compute and integrate the learning rules of the parameters of the first order lowpass filter, gain and time constant. Section 2.3 presents simulation results with HSPICE using BSIM3v3 models for a 0.5μm technology. The gain and time constant parameters adapt quickly and stably, and the error between the outputs of the adaptive estimator and the unknown system approaches zero when adaptation is completed. Section 2.4 describes testing results and mismatch analysis for the system. Experimental results agree well with the simulation results and further verify the validity of the learning rules.

2.1 Derivation of Learning Rules

We describe control laws for a tunable filter which address the classical problem of system identification, depicted in Figure 2.1: an input signal is applied to both an unknown system *(plant)* and to an adaptive estimator *(model)* system which estimates the parameters of the unknown plant. The difference between the plant and the model, the error, is used to adjust the parameters. We design the adaptive laws for adjusting the

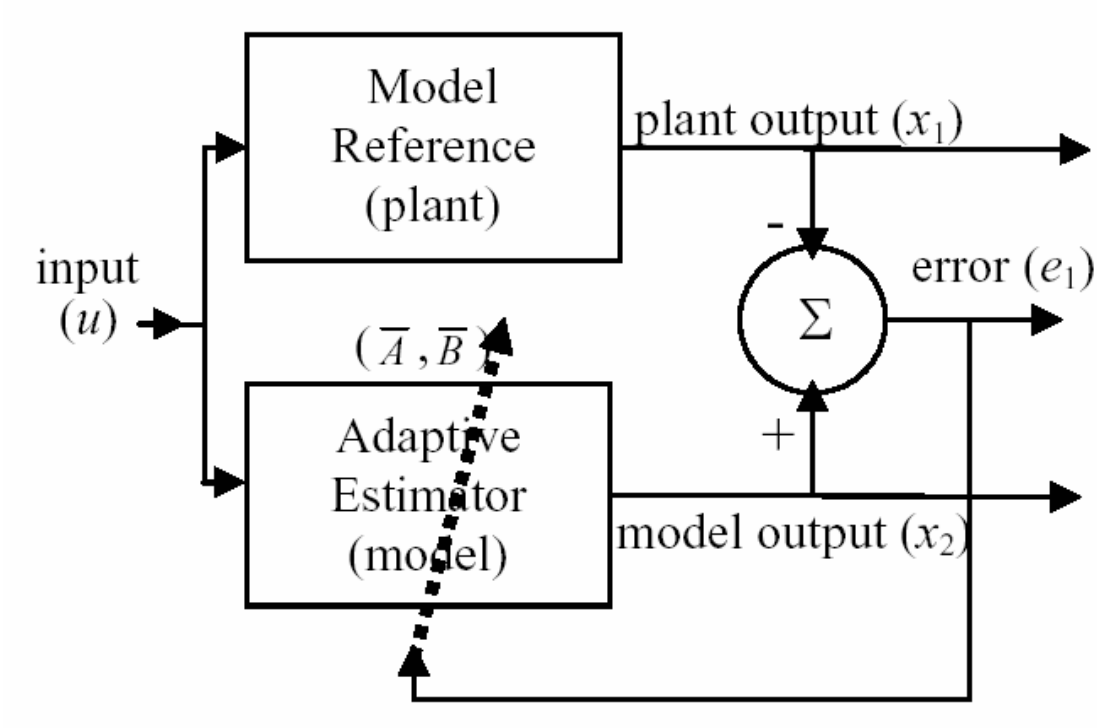

Figure 2.1: The system identification problem: an input *u* is applied to both plant and model filters. The error e_1 is the difference of plant and model outputs $(x_2 - x_1)$ and is used to adapt the parameters of the model $(\overline{A}, \overline{B})$.

control parameters so as to ensure stability of the learning procedure.

The unknown plant and the adaptive model filters are described by the state-variable representation:

$$\dot{x}_1 = -Ax_1 + ABu \qquad \text{plant output} \qquad (2.1)$$

$$\dot{x}_2 = -\overline{A}x_2 + \overline{A}\overline{B}u \qquad \text{model output} \qquad (2.2)$$

where x_1 is the output of the plant, A is the reciprocal of the plant time constant, B is the plant gain, u is the input to both filters, x_2 is the output of the model, $\overline{A}$ is the estimate of the reciprocal time constant, and $\overline{B}$ is the estimate of the gain.

In order to assess the performance and stability of the adaptation, we construct the error system as the differences between plant and model outputs, between estimated and true reciprocal time constant, and between estimated and true gain:

$$e_1 = x_2 - x_1 \qquad \text{output error} \qquad (2.3)$$

$$e_2 = \overline{A} - A \qquad \text{(1/time constant) error} \qquad (2.4)$$

$$e_3 = \overline{B} - B \qquad \text{gain error} \qquad (2.5)$$

We are interested in adaptive laws controlling system parameters so that all errors tend towards zero with time. Thus we can focus on the essential features of the control problem by considering the dynamics of the error system:

$$\dot{e}_1 = \dot{x}_2 - \dot{x}_1 \qquad (2.6)$$

$$\dot{e}_2 = \dot{\overline{A}} \qquad (2.7)$$

$$\dot{e}_3 = \dot{\overline{B}} \qquad (2.8)$$

The dynamics of the output error are determined by the system, but we have the flexibility to specify the dynamics of the parameter errors so that the control laws drive the estimates stably to their true values.

We employ the direct method of Lyapunov to investigate the stability of the adaptive system and to derive appropriate control laws [13]. We choose a suitable scalar function and examine the temporal derivative of this function along trajectories of the system. A Lyapunov function must satisfy the following three conditions: positive definite, negative definite time derivative, and radially unbounded. For system identification of the first order low-pass filter we consider the Lyapunov function:

$$V(e) = \frac{1}{2}\left(e_1^2 + e_2^2 + e_3^2\right) \tag{2.9}$$

This function satisfies the first and third conditions and has the following temporal derivative, evaluated in terms of the simple adaptive system described above:

$$\begin{aligned}
\dot{V}(e) &= e_1\dot{e}_1 + e_2\dot{e}_2 + e_3\dot{e}_3 \\
&= e_1\left[\left(-\overline{A}x_2 + \overline{A}\overline{B}u\right) - \left(-Ax_1 + ABu\right)\right] + e_2\dot{e}_2 + e_3\dot{e}_3 \\
&= e_1\left[-\left(A + e_2\right)x_2 + \left(A + e_2\right)\left(B + e_3\right)u + A\left(x_2 - e_1\right) - ABu\right] + e_2\dot{e}_2 + e_3\dot{e}_3 \\
&= e_1\left[-e_2x_2 + e_2\overline{B}u + e_3Au - Ae_1\right] + e_2\dot{e}_2 + e_3\dot{e}_3 \\
&= -Ae_1^2 + e_1e_2\left(-x_2 + \overline{B}u\right) + e_1e_3Au + e_2\dot{e}_2 + e_3\dot{e}_3 \\
&= -Ae_1^2 + e_1e_2\frac{\dot{x}_2}{\overline{A}} + e_1e_3Au + e_2\dot{e}_2 + e_3\dot{e}_3
\end{aligned} \tag{2.10}$$

Note that the control laws for the time constant and gain errors ($\dot{e}_2$ and $\dot{e}_3$ respectively) remain unspecified, and we choose them to satisfy the second condition for the Lyapunov function. There are multiple solutions which provide such a negative time derivative:

$$\dot{V}(e) = -Ae_1^2 \tag{2.11}$$

We choose the following pair of control laws:

$$\dot{e}_2 = -e_1 \frac{\dot{x}_2}{\overline{A}} \tag{2.12}$$

$$\dot{e}_3 = -e_1 A u \tag{2.13}$$

These rules may be simplified further since in current mode log domain filters, many system variables are strictly positive, including the estimate of the reciprocal time constant $\overline{A}$, the true reciprocal time constant A, and the input u. Multiplying the rules by a positive scalar factor affects the rate of adaptation, but not the direction. Thus we can express the control laws simply:

$$\dot{e}_2 \propto -e_1 \dot{x}_2 \tag{2.14}$$

$$\dot{e}_3 \propto -e_1 \tag{2.15}$$

In our implementation the estimate of the reciprocal time constant is provided by integrating the product of the output error with the temporal derivative of the model output, and the estimate of the gain is provided by integrating the output error.

We multiply two positive factors C and D to both learning rules and rewrite the new time derivative of the Lyapunov function as follows:

$$\begin{aligned} \dot{V}(e) &= e_1\dot{e}_1 + e_2\dot{e}_2 + e_3\dot{e}_3 \\ &= -Ae_1^2 + e_1 e_2 \frac{\dot{x}_2}{\overline{A}} + e_1 e_3 A u + e_2\dot{e}_2 + e_3\dot{e}_3 \\ &= -Ae_1^2 + e_1 e_2 \frac{\dot{x}_2}{\overline{A}} + e_1 e_3 A u + e_2\left(-Ce_1\dot{x}_2\right) + e_3\left(-De_1\right) \\ &= -Ae_1^2 + e_2 e_1 \dot{x}_2\left(\frac{1}{\overline{A}} - C\right) + e_1 e_3\left(Au - D\right) \end{aligned} \tag{2.16}$$

Even if $\overline{A}$ and Au are not constants and we cannot tune C and D to cancel them exactly at all the time, we can at least ensure that the parameters are updated in the correct direction so that they approach the final desired adaptation state. The learning

procedure may not be optimal, but the estimator will eventually adapt to the unknown system since the learning rules are in the right direction.

2.2 Circuit Implementation

To demonstrate the learning rules we have derived using the Lyapunov method in the above section, we construct circuits implementing a first order lowpass filter model and integrating these learning rules for adaptation of the time constant and gain.

2.2.1 MITE Implementation of Log Domain First Order Lowpass filters

Log domain filters are a dynamic extension of classical static translinear circuits. They offer wide tuning range, large dynamic range, and low voltage / low power operation. The circuit in Figure 2.2(a) is the first order lowpass filter with cascode transistors used as an unknown plant and Figure 2.2(b) is the corresponding implementation for the adaptive model.

In subthreshold operation the MITE current is an exponential function of the summed inputs:

$$I_1 = I_0 e^{K(V_1 + V_{g\_ref})} = I_{in} \tag{2.17}$$

$$I_2 = I_0 e^{K(V_1 + V_2)} \tag{2.18}$$

$$I_3 = I_0 e^{K(V_2 + V_3)} = I_\tau \tag{2.19}$$

$$I_4 = I_0 e^{K(V_3 + V_{gain})} = I_{out} \tag{2.20}$$

M1, M2, M3 and M4 form a translinear loop, so the current I_2 can be expressed as:

$$I_2 = \frac{I_{in} I_\tau}{I_{out}} e^{K(V_{gain} - V_{g\_ref})} \tag{2.21}$$

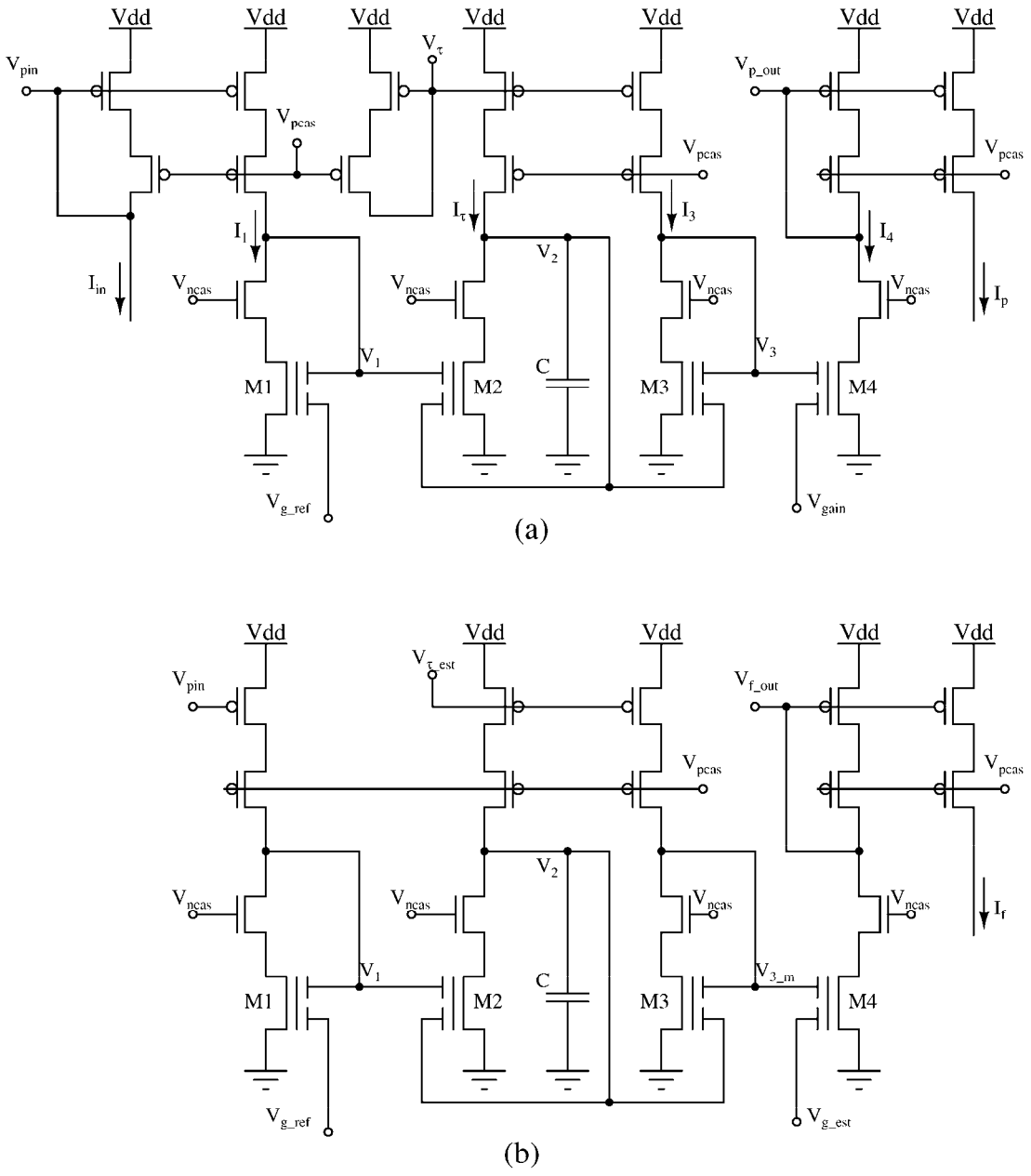

Figure 2.2: (a) Log domain MITE filter for a first order lowpass transfer function used as the unknown plant; (b) Log domain MITE implementation for adaptive model.

We apply Kirchoff's Current Law (KCL) at the capacitive node to find the relationship between the MITE currents and the capacitive current:

$$C\dot{V}_2 + I_2 = I_\tau = C\dot{V}_2 + \frac{I_{in} I_\tau}{I_{out}} e^{K(V_{gain} - V_{g\_ref})} \qquad (2.22)$$

Since V_2 and V_3 together control a constant current I_3, their time derivatives are opposite in sign but equal in magnitude:

$$\dot{I}_3 = I_3 \cdot K(\dot{V}_2 + \dot{V}_3) = 0 \Rightarrow \dot{V}_3 = -\dot{V}_2 \qquad (2.23)$$

We determine the transfer function for the output current I_{out} by differentiating it, then substituting our results from the KCL and MITE relationships above:

$$\dot{I}_{out} = I_{out} K\dot{V}_3 = -I_{out} K\dot{V}_2 = -KI_{out} \frac{I_\tau}{C}\left[1 - \frac{I_{in}}{I_{out}} e^{K(V_{gain} - V_{g\_ref})}\right]$$

$$\dot{I}_{out} = \frac{KI_\tau}{C}\left[-I_{out} + I_{in} e^{K(V_{gain} - V_{g\_ref})}\right] \qquad (2.24)$$

which is a first order low-pass transfer function with time constant $\tau = C / KI_\tau$ and gain $e^{K(V_{gain} - V_{g\_ref})}$. The time constant is the ratio between capacitance and bias current, easily tuned by adjusting the bias current. The gain is the exponential of the voltage difference between V_{gain} and V_{g_ref}, easily tuned by adjusting the voltage V_{gain}.

2.2.2 MITE Implementation of Learning Rules

The plant and model are first order lowpass filters, each with two adjustable parameters: gain and the reciprocal of the time constant. We have implemented learning rules derived using the Lyapunov method described in section 2.1. The inputs to the learning rules are the system output error and the temporal derivative of the model output.

The temporal derivative of the model output is computed using the circuit shown in Figure 2.3: A wide range OTA (Operational Transconductance Amplifier) operates as a voltage follower with a capacitor connected to the output, with current $I_d = I_{d1} - I_{d2}$. Suppose transistors M1 and M2 in Figure 2.3 are well matched and have the same transconductance g_m. Since I_{d1} and I_{d2} are mirrored from the drain currents of M1 and M2 respectively, their difference can be expressed as

$$I_d = I_{d1} - I_{d2} = g_m(V_1 - V_2) = C_d \dot{V}_2$$

$$\Rightarrow V_2 = \frac{g_m}{g_m + sC_d} V_1 \qquad (2.25)$$

$$I_d = g_m \left(V_1 - \frac{g_m}{g_m + sC_d} V_1 \right) = \frac{sC_d V_1}{1 + sC_d / g_m} \qquad (2.26)$$

When $g_m >> sC_d$, the output current is approximately the derivative of the input voltage $I_d \approx sC_d V_1 = SC_d I_f R$. To make the transconductance g_m large, we operate the input devices near threshold. It is not necessary to explicitly convert the filter output current into voltage; we use intermediate node voltage V_{3_m} of Figure 2.2(b) directly as input to the temporal derivative computation. This eliminates resistance R, so loading on the node V_3 is minimal. Note that since $\dot{I}_f = I_f K \dot{V}_3$, the adaptation rule becomes $\dot{e}_2 \propto (I_p - I_f)\dot{I}_f / KI_f$. Input nodes nd1yank and nd2yank in Figure 2.3 control two NMOS transistors which subtract part of the currents from I_{d1} and I_{d2} respectively to compensate mismatch in the system. I'_{d1} and I'_{d2} are passed on to the next circuit stage.

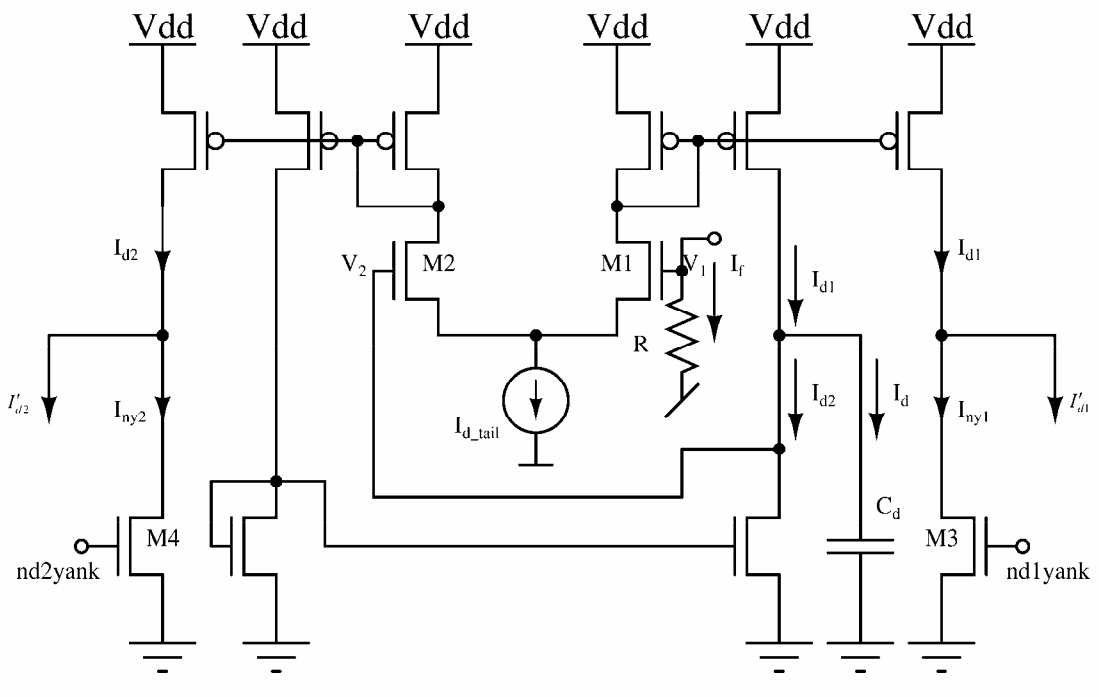

Figure 2.3: Circuit for computing temporal derivative with mismatch controllers.

The time constant learning rule requires a four quadrant multiplication, also implemented using a MITE circuit shown in Figure 2.4 with inputs I'_{d1}, I'_{d2}, I_p and I_f and outputs I_{nm1} and I_{nm2}. Transistor groups (M1, M2, M4, M6), (M1, M2, M5, M7), (M1, M3, M4, M8) and (M1, M3, M5, M9) form four translinear loops which give:

$$I_6 = I_f I'_{d2} / I_{bias} \tag{2.27}$$

$$I_7 = I_f I'_{d1} / I_{bias} \tag{2.28}$$

$$I_8 = I_p I'_{d2} / I_{bias} \tag{2.29}$$

$$I_9 = I_p I'_{d1} / I_{bias} \tag{2.30}$$

If we apply KCL at nodes I_{nm1} and I_{nm2}, the difference between the currents flowing in the two nodes can be expressed as:

$$\begin{aligned} I_{nm1} - I_{nm2} &= \left(I_6 + I_9\right) - \left(I_7 + I_8\right) \\ &= \left(I_f I'_{d2} + I_p I'_{d1}\right) / I_{bias} - \left(I_f I'_{d1} + I_p I'_{d2}\right) / I_{bias} \\ &= \left(I_p - I_f\right)\left(I'_{d1} - I'_{d2}\right) / I_{bias} \end{aligned} \tag{2.31}$$

The update direction for time constant of the first order lowpass filter $\dot{e}_3 \propto -e_1 \dot{x}_2$ is given by the current difference between I_{nm1} and I_{nm2}.

Schematics for the learning rules and summing nodes are shown in Figure 2.5: panel (a) shows the integrator for gain adaptation; panel (b) shows the integrator and differential pair for time constant adaptation. The cascode arrangement is used in all current mirrors to minimize early effect and increase trans-amp gain.

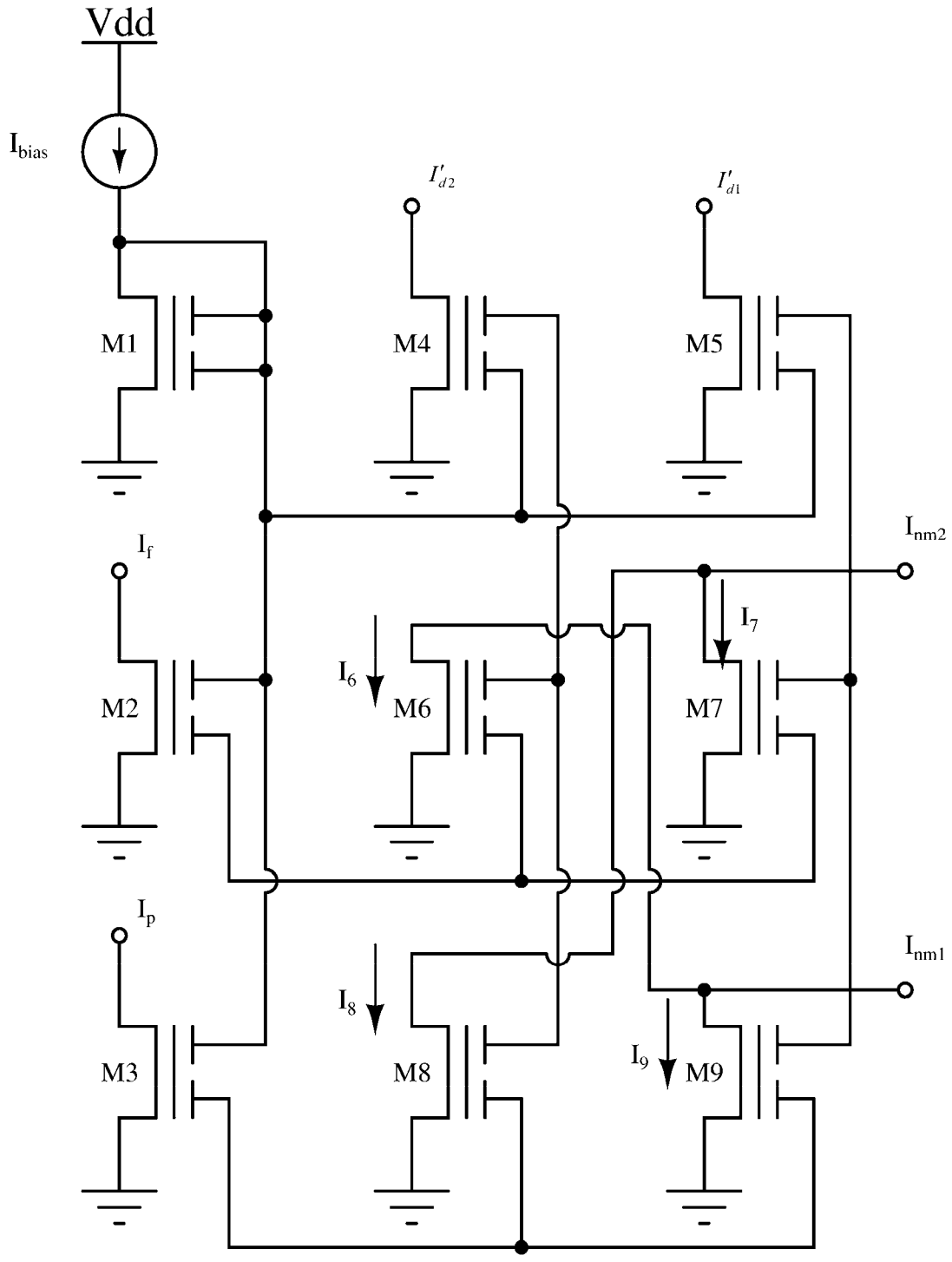

Figure 2.4: Circuit for four quadrant multiplication.

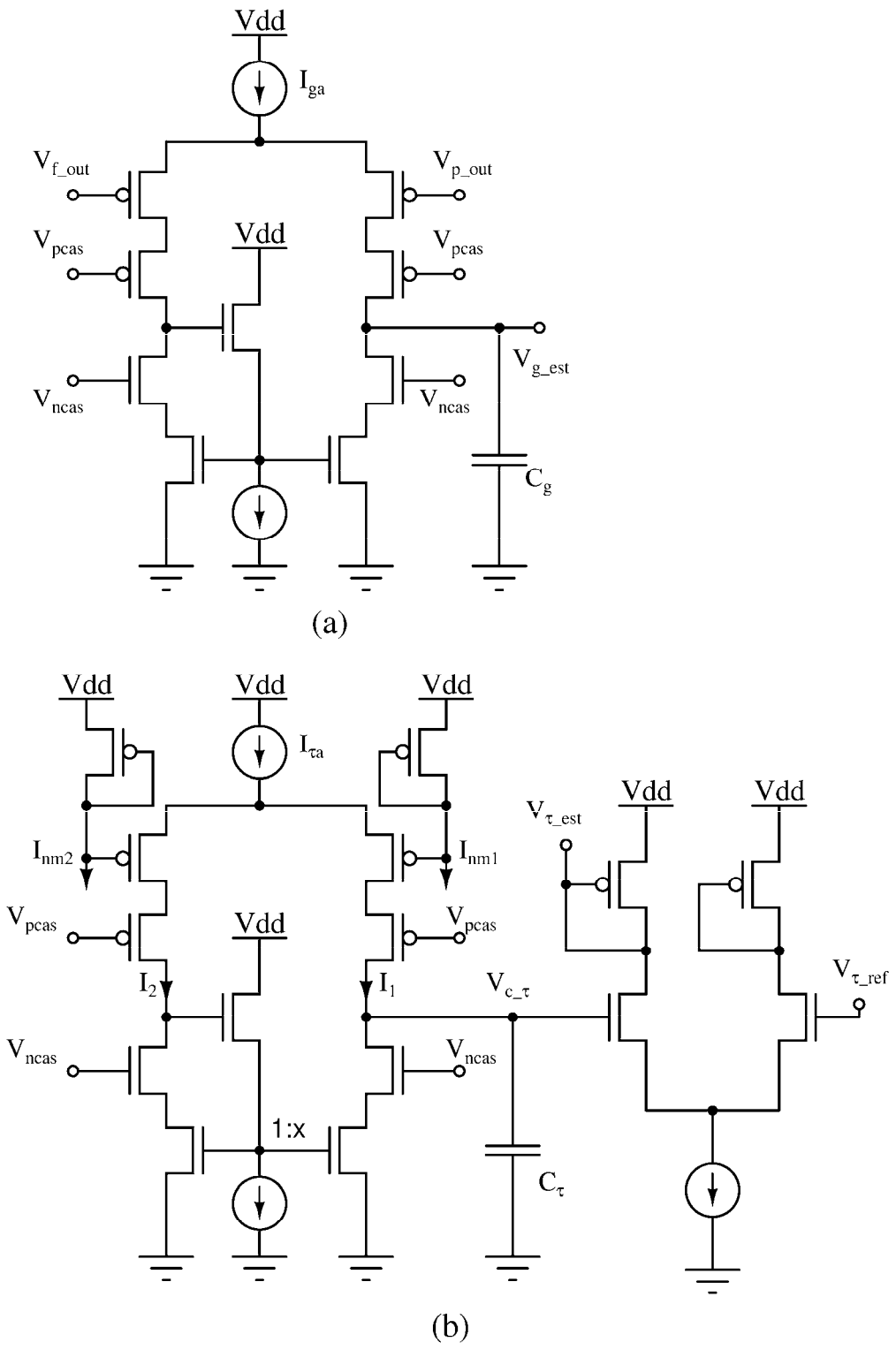

Figure 2.5: MITE implementation of learning rules for gain and time constant.

2.3 Simulation Results

We simulate the circuit with HSPICE using BSIM3v3 models for a 0.5μm technology. We use the technique in [14] to avoid floating-node problems in the simulator. A schematic diagram illustrating this technique is shown in Figure 2.6. We add a voltage-dependent voltage source $V_{floating\_gate}$ from ground to the floating gate through a big resistor R. There is no current through R, because $V_{floating\_gate}$ tracks the floating gate voltage itself. This artificial DC path to ground aids numerical convergence in the HSPICE circuit simulator. We use a square wave (Figure 2.7), harmonic sine waves (Figure 2.8), and equally spaced sine wave frequencies (Figure 2.9) as inputs.

Figure 2.7 shows adaptation with a $10kHz$ square wave. The square wave pulses from $20nA$ to $160nA$. Figure 2.7 (a) is the error I_e between the plant and filter outputs. Figure 2.7 (b) shows V_τ and V_{τ_est}. Figure 2.7 (c) shows V_{gain} and V_{g_est}. We intentionally vary the time constant of the plant (by a factor of 16) and the gain to see how well the filter adapts. The different V_τ values correspond to I_τ of $40nA$ from $0 \sim 2ms$, $80nA$ from $2 \sim 3.5ms$, $20nA$ from $3.5 \sim 5ms$, $160nA$ from $5 \sim 6.5ms$, and $10nA$ from $6.5 \sim 8ms$. The voltage V_{gain} is changed as 1.4V from $0 \sim 1ms$, 1.5V from $1 \sim 2.5ms$, 1.35V from $2.5 \sim 4ms$, and linearly increases from 1.4V to 1.5V from $4 \sim 5.5ms$, and linearly decreases from 1.5V to 1.45V from $5.5 \sim 7.5ms$, and keeps constant at 1.45V from $7.5 \sim 8ms$. For all changes in V_τ and V_{gain}, V_{τ_est} and V_{g_est} accurately track the new values respectively. $I_e \to 0$ when $V_{\tau\_est} \to V_\tau$ and $V_{gain} \to V_{g\_est}$. V_{g_ref} is fixed at 1.5V. The adaptation rate depends on signal strength,

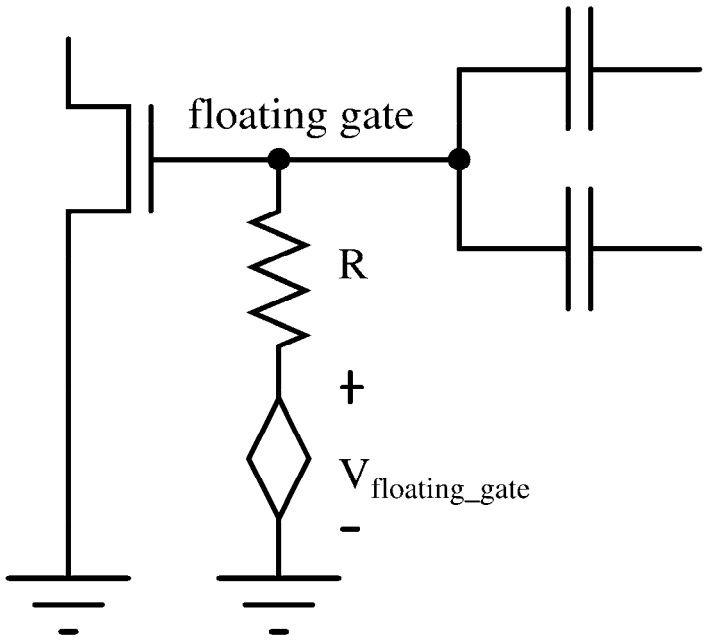

Figure 2.6: Technique used to avoid floating-node problems in the simulator.

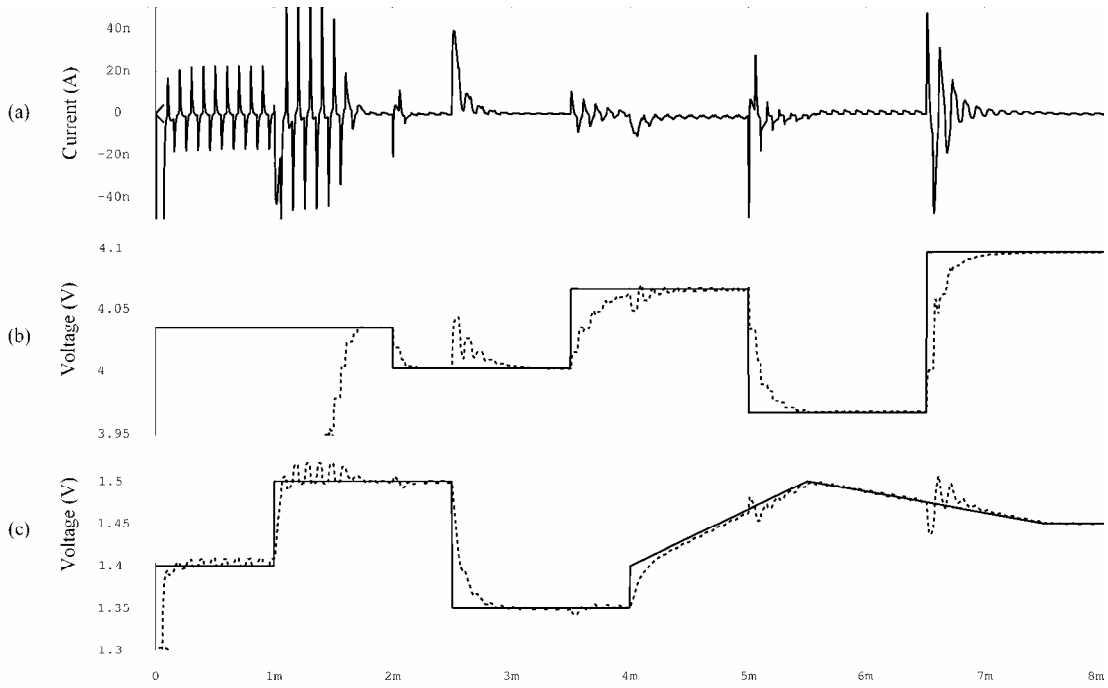

Figure 2.7: Adapting with a 10kHz square wave input.

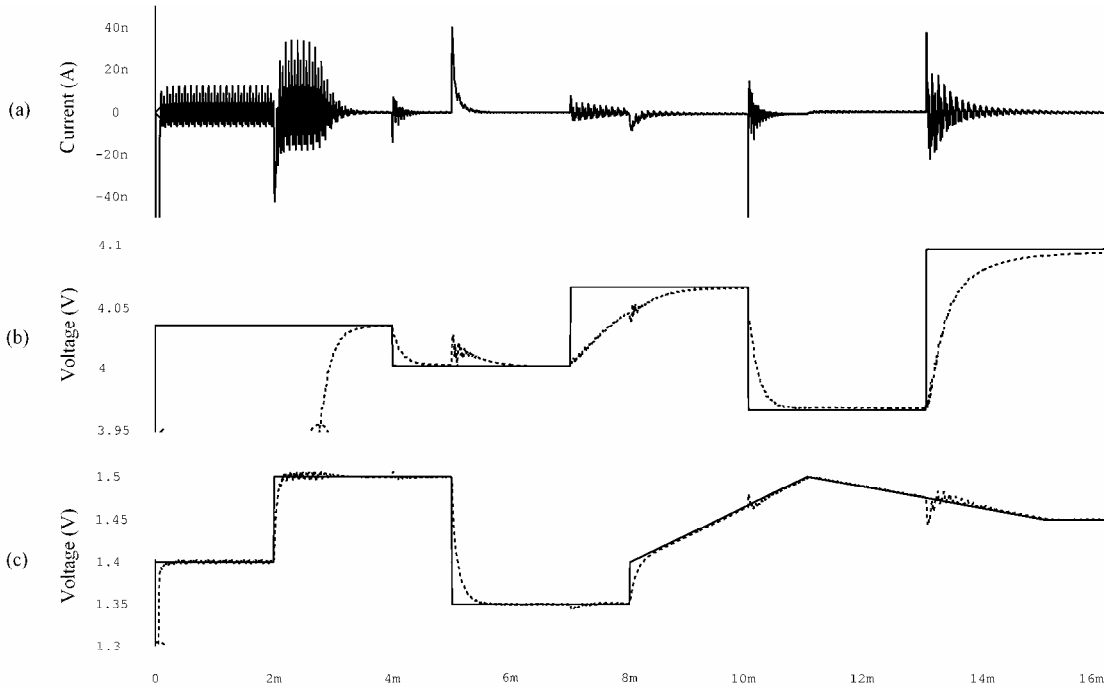

Figure 2.8: Adapting with 4 harmonic sine waves.

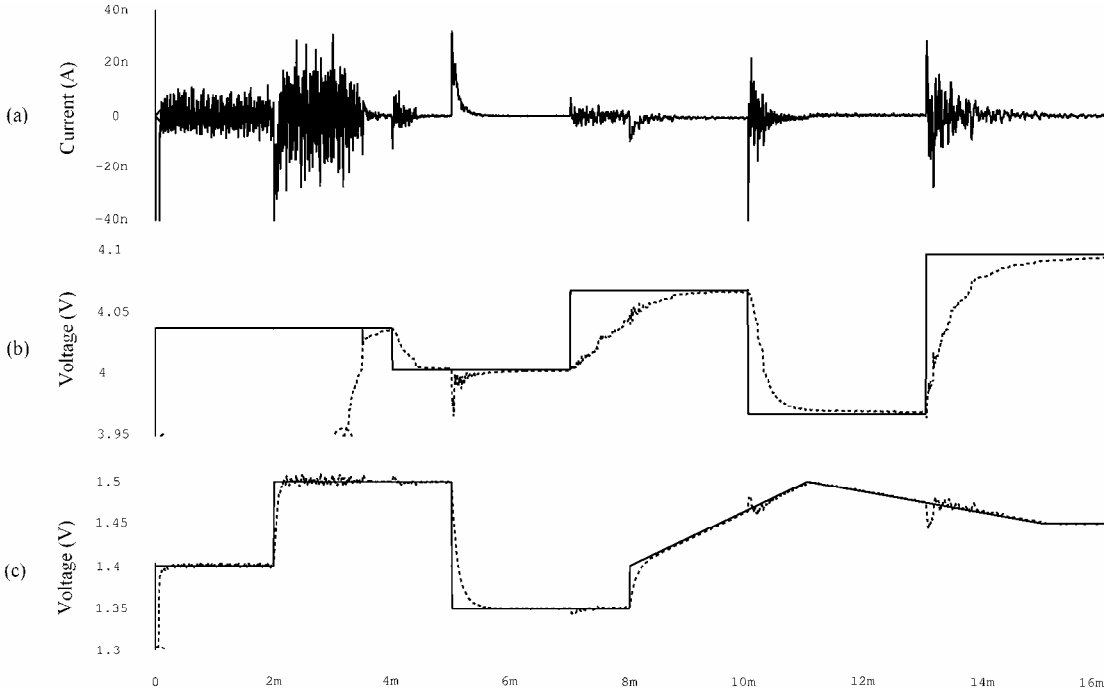

Figure 2.9: Adapting with 14 geometrically spaced sine waves from 5-97kHz.

currents I_{ga} and $I_{\tau a}$, and capacitors C_g and C_τ.

Next, we show the adaptation when the signal is a mixture of sine waves. In Figure 2.8 (a)-(c) we use a combination of sine waves equally weighted at $10kHz$, $20kHz$, $40kHz$, and $80kHz$ as input. The input signal is biased at 90nA and has a 40nA peak to peak oscillation for each frequency. In Figure 2.9(a)-(c) the input is a summation of 14 sine waves, whose frequency ratio is an irrational number $2\pi/5$, spanning from $5kHz$ to $97kHz$. The input signal is also biased at 90nA and has a 10nA peak to peak oscillation for each frequency. For those two very different inputs, V_{τ_est} accurately tracks V_τ [Figure 2.8(b) and Figure 2.9(b)] and V_{g_est} tracks V_{gain} [Figure 2.8(c) and Figure 2.9(c)], and I_e approaches zero when adaptation is completed.

2.4 Experimental Results

We present measurements from a first order adaptive filter designed and fabricated in 0.5μm CMOS technology (AMI 0.5μm run T38O). The plant and the filter in Figure 2.2 are implemented using transistors with a W/L ratio of 12/6. The input current and the output currents that flow in these parts of circuit have to be around or below $100nA$, in order for all the transistors to operate in subthreshold. To implement these tiny currents, a 100:1 current mirror is used in the input stage shown in Figure 2.10 to raise the input current of the chip up to $10\mu A$. A Howland current source [15] with resistor values of $R_1 = R_2 = R_3 = R_4 = 97.6k\Omega$ shown in Figure 2.10 is used off-chip to convert the input voltages to input currents. There are no currents flowing into both the positive and negative nodes of the op-amp. The voltages of these two nodes are identical as follows if we assume infinite gain of the op-amp.

$$V_- = V_+ = \frac{R_4}{R_1 + R_4} V_{out} + \frac{R_1}{R_1 + R_4} V_{in} \tag{2.32}$$

To apply KCL at the node V_-, the input current to the chip can be expressed as:

$$\begin{aligned} I_{in} &= \frac{V_{out} - V_-}{R_3} - \frac{V_-}{R_2} \\ &= \frac{1}{R_3}\left(1 - \frac{R_2 + R_3}{R_2} \cdot \frac{R_1}{R_1 + R_4}\right) V_{out} - \frac{R_2 + R_3}{R_2 R_3} \cdot \frac{R_4}{R_1 + R_4} V_{in} \end{aligned} \tag{2.33}$$

If the relations among R_1, R_2, R_3 and R_4 satisfies

$$\frac{R_3}{R_2} = \frac{R_4}{R_1} \tag{2.34}$$

Equation (2.33) can be rewritten as:

$$I_{in} = -\frac{V_{in}}{R_2} \tag{2.35}$$

Thus, a linear relation between input voltage and the current is achieved. We can easily present input signals using a standard function generator or a PC-controlled DAC card. Two identical current conveyors with a 1390:6 current ratio as shown in Figure 2.10 are used in the output stage for the same reason. Two TL084 JFET-input operational amplifier are used with a $100k\Omega$ resistor and a 100μF capacitor in parallel in the negative feedback path and bias the positive input node at 2.5V to convert the output currents to output voltages, which makes it easy to measure with an oscilloscope or appropriate data acquisition card. The capacitors are used to attenuate the high frequency noise for the output voltages. The relation between output voltages (V) and output currents (μA) can be expressed as:

$$\begin{aligned} V_{pl\_out} &\approx 2.5 + 0.1 \cdot I_{p\_out} \\ V_{filt\_out} &\approx 2.5 + 0.1 \cdot I_{filt\_out} \end{aligned} \tag{2.36}$$

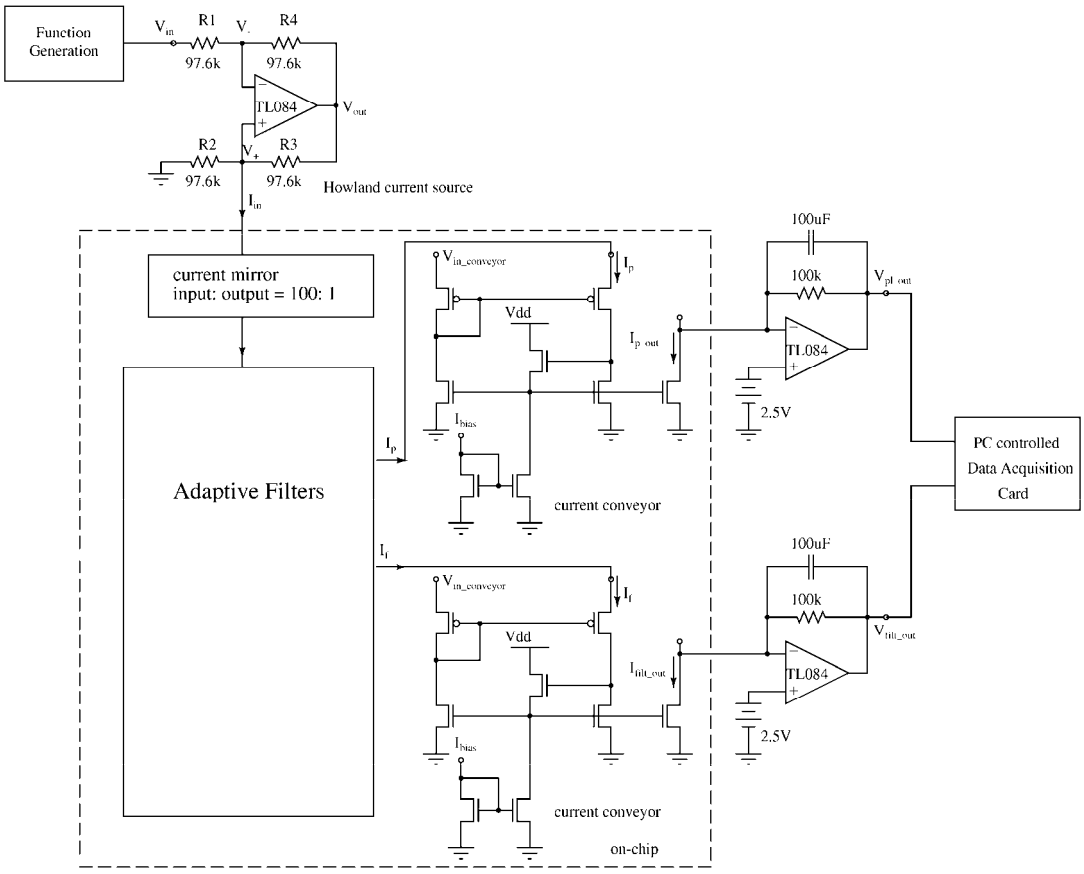

Figure 2.10: Testing setup for the adaptive first order lowpass filters including schematics of input voltage-current converter Howland current source, on-chip current conveyors, and output current-voltage converters.

We use a $10kHz$ square wave with amplitude of $0.2V$ and bias of $0.3V$ as the input voltage to the system, which is converted by the off-chip Howland current source and on-chip current mirrors to an input current with peak to peak amplitude of $80nA$ and bias of $60nA$. If the mismatch in the learning rules is adjusted appropriately using nd1yank and nd2yank, the error between the plant and model outputs does not exceed 4% of the plant output for fixed values of gain and time constant. We intentionally vary the gain and time constant of the plant to see how well the filter adapts. Figure 2.11(a) shows the error between the plant and model outputs. Figure 2.11(b) shows the gain control voltages V_{gain} and V_{g_est} for plant and model. Figure 2.11(c) shows the time constant control voltages V_{τ} and V_{τ_est}. For all the changes in V_{gain} and V_{τ}, we observe accurate adaptation of V_{g_est} and V_{τ_est}. The measured power consumption of the circuits is about 33μW. We observe a constant voltage difference of magnitude 0.07V between V_{gain} and V_{g_est}, which has been subtracted from the voltage V_{gain} shown in Figure 2.11(b). This constant voltage difference results from different amounts of stored charge on the floating gates in the plant and model filters. Figure 2.12 and Figure 2.13 show testing results for two different chips over a longer time period than Figure 2.11, which demonstrate the interaction between adaptation of gain and time constant. All the input conditions are as same as above. The constant voltage difference has not been subtracted for either case. Figure 2.12(a) and Figure 2.13(a) show the gain control voltages V_{gain} and V_{g_est} for plant and model. Figure 2.12(b) and Figure 2.13(b) show the time constant control voltages V_{τ} and V_{τ_est}. In the following section we present a mismatch analysis which accounts for the small difference between V_{τ} and V_{τ_est}.

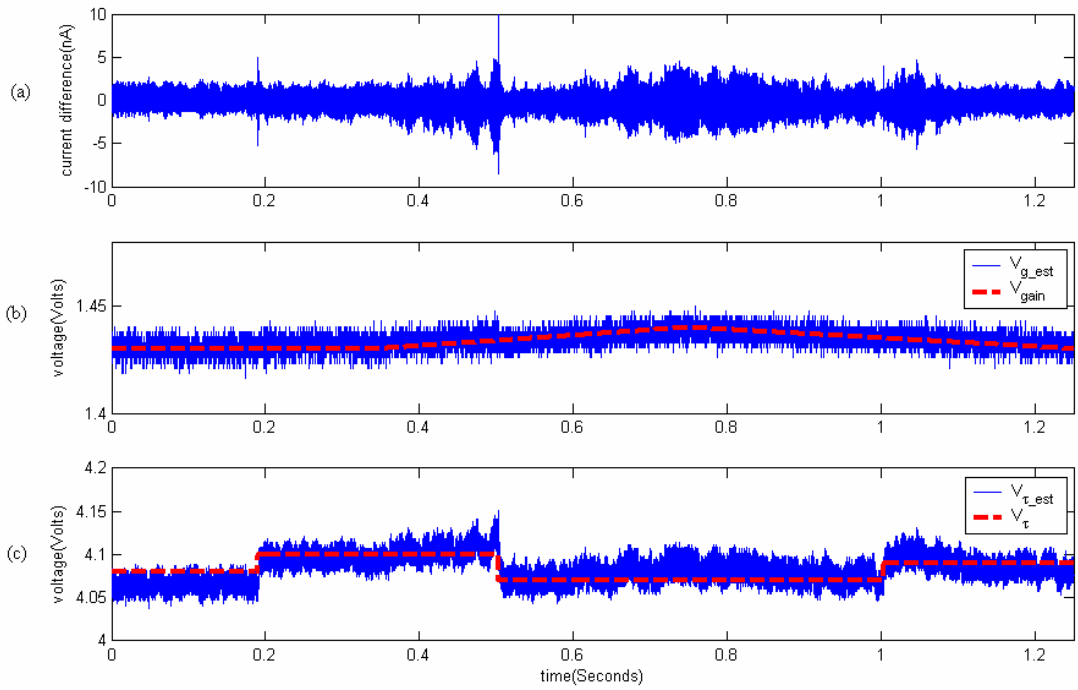

Figure 2.11: Testing results of adaptation process: (a) error of outputs of plant and model filters. (b) gain control voltages of plant and model filters. (c) time constant control voltages of plant and model filters.

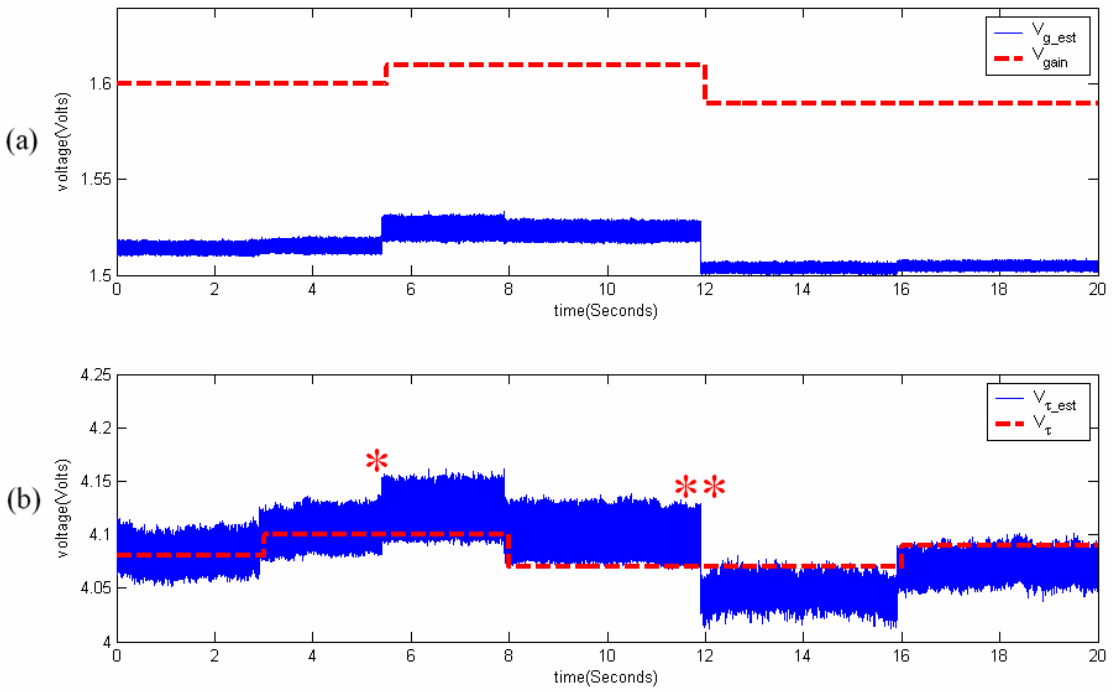

Figure 2.12: Testing results of adaptation process: changes of gain voltages and time constant voltages to demonstrate condition 2 in mismatch analysis.

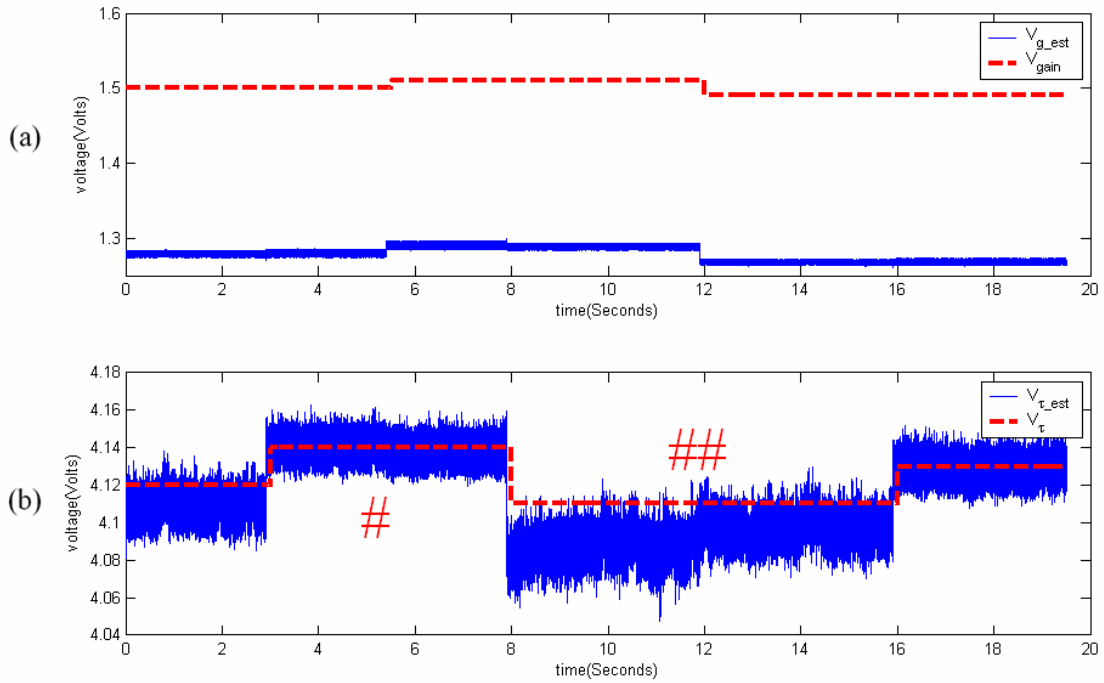

Figure 2.13: Testing results of adaptation process: changes of gain voltages and time constant voltages to demonstrate condition 3 in mismatch analysis.

2.5 Analysis of Current Mirror Ratio Mismatch and Compensation

Consider the implementation of the time constant learning rule shown in Figure 2.5(b). Ideally, without the mismatch compensation we have

$$\begin{aligned} I_1 &= c\left(I_p I_{d1} + I_f I_{d2}\right)/ I_{bias} \\ I_2 &= c\left(I_p I_{d2} + I_f I_{d1}\right)/ I_{bias} \end{aligned} \tag{2.37}$$

Suppose the mismatch of this circuit is limited to mismatch in the current mirror ration, so that the actual ratio is $1:x$, where the ideal ratio is 1:1 and x is a constant around 1. The non-ideal currents $I_1^{'}$ and $I_2^{'}$ correspond to the ideal currents I_1 and I_2 can be written as:

$$\begin{aligned} I_1^{'} &= c'\left[I_p\left(I_{d1} - I_{ny1}\right) + I_f\left(I_{d2} - I_{ny2}\right)\right]/ I_{bias} \\ I_2^{'} &= c'\left[I_p\left(I_{d2} - I_{ny2}\right) + I_f\left(I_{d1} - I_{ny1}\right)\right]/ I_{bias} \end{aligned} \tag{2.38}$$

where I_{ny1} is the current flowing in NMOS transistor M3 to ground and I_{ny2} is the current flowing in NMOS transistor M4 to ground for the temporal derivative circuit shown in Figure 2.3. Since $I_{\tau a} = I_1 + I_2 = I_1^{'} + I_2^{'}$ is a constant shown in Figure 2.5(b), we obtain

$$c' = \frac{I_{d\_tail}}{I_{d\_tail} - I_{ny1} - I_{ny2}} c \tag{2.39}$$

$$I_{d\_tail} = I_{d1} + I_{d2} \tag{2.40}$$

The current I_{d_tail}, which is the sum of I_{d1} and I_{d2}, is also a constant. If we further assume that the time required for the time for adaptation t_0 is the same in both cases, and

that the mismatch compensation provided by M3 and M4 works well enough to ensure that both cases converge to the same voltage integrated on the same capacitor, we obtain

$$\int_0^{t_0}(I_1 - I_2)dt = \int_0^{t_0}(I_1{}' - xI_2{}')dt \qquad (2.41)$$

Since I_{ny1} and I_{ny2} are currents flowing in NMOS transistor from a higher voltage to ground, they cannot be negative. There are only four possible cases for them, outlined as follows:

1. $I_{ny1} = 0 \quad I_{ny2} = 0$

2. $I_{ny1} = 0 \quad I_{ny2} > 0$

3. $I_{ny1} > 0 \quad I_{ny2} = 0$

4. $I_{ny1} > 0 \quad I_{ny2} > 0$

Case 1 is the ideal situation in which there is no mismatch in the system and no mismatch compensation is required.

Case 2 has not been observed in testing any of the chips.

Cases 3 and 4 are observed in all the chips tested thus far.

For simplicity of analysis, we only consider Case 3: $I_{ny1} > 0 \quad I_{ny2} = 0$. Since $(I_{d1} - I_{ny1}) - (I_{d2} - I_{ny2}) = (I_{d1} - I_{d2}) + (I_{ny2} - I_{ny1})$ is applied as the derivative in later stages, we can compensate for $I_{ny2} > 0$ by increasing I_{ny1}. Substituting the currents of equations (2.37) and (2.38) into equation (2.41), we can calculate the current (for $I_{ny2} = 0$) which can compensate the current mirror ratio mismatch of $1 : x$ we assumed at the beginning.

$$\begin{aligned}&\left(I_{d\_tail}-I_{ny1}\right)\int_0^{t_0}\left(I_pI_{d1}+I_fI_{d2}-I_pI_{d2}-I_fI_{d1}\right)dt\\&=I_{d\_tail}\int_0^{t_0}\left(I_pI_{d1}-I_pI_{ny1}+I_fI_{d2}-xI_pI_{d2}-xI_fI_{d1}+xI_fI_{ny1}\right)dt\end{aligned}\tag{2.42}$$

$$I_{d\_tail}\int_0^{t_0}(x-1)\left(I_pI_{d2}+I_fI_{d1}\right)dt=I_{ny1}\left[I_{d\_tail}\int_0^{t_0}\left(xI_f-I_p\right)dt+\int_0^{t_0}\left(I_p-I_f\right)\left(I_{d1}-I_{d2}\right)dt\right]\tag{2.43}$$

$$\begin{aligned}I_{ny1}&=\frac{I_{d\_tail}\int_0^{t_0}(x-1)\left(I_pI_{d2}+I_fI_{d1}\right)dt}{I_{d\_tail}\int_0^{t_0}\left(xI_f-I_p\right)dt+\int_0^{t_0}\left(I_p-I_f\right)\left(I_{d1}-I_{d2}\right)dt}\\&=\frac{I_{d\_tail}\int_0^{t_0}(x-1)\frac{I_2I_{bias}}{c}dt}{I_{d\_tail}\int_0^{t_0}\left(xI_f-I_p\right)dt+\int_0^{t_0}\frac{\left(I_1-I_2\right)I_{bias}}{c}dt}\\&=\frac{I_{d\_tail}I_{bias}\frac{x-1}{2}\left[\int_0^{t_0}I_{\tau a}dt-\int_0^{t_0}\left(I_1-I_2\right)dt\right]}{cI_{d\_tail}\int_0^{t_0}\left(xI_f-I_p\right)dt+I_{bias}\int_0^{t_0}\left(I_1-I_2\right)dt}\end{aligned}\tag{2.44}$$

Since $I_{\tau a}$ is a constant current, its integral $\int_0^{t_0}I_{\tau a}dt=I_{\tau a}t_0$ is also a constant. The current difference $\left(I_1-I_2\right)$ controls the capacitor voltage, which controls the time constant of the first order low pass filter. Assuming the initial capacitor voltage is 0V, then $\int_0^{t_0}\left(I_1-I_2\right)dt=C_\tau V_{c\_\tau}$, where C_τ is the capacitance, and V_{c_τ} ,which is the voltage on the capacitor, controls the estimated time constant control voltage V_{τ_est} as shown in Figure 2.5(b). V_{τ_est} will decrease as V_{c_τ} increases, and will increase as V_{c_τ} decreases.

If we approximate $\int_0^{t_0} I_p dt = \int_0^{t_0} I_f dt = I_b t_0$ as a constant, we obtain

$$I_{ny1} = \frac{(x-1)I_{d\_tail}}{2} \cdot \frac{\frac{I_{\tau a} t_0}{C_t} - V_{c\_\tau}}{\frac{cI_d}{I_{bias} C_t}(x-1)I_b t_0 + V_{c\_\tau}} = X \cdot \frac{Y - V_{c\_\tau}}{Z + V_{c\_\tau}} \qquad (2.45)$$

where X, Y, and Z are defined as $X \equiv \frac{(x-1)I_{d\_tail}}{2}$ $Y \equiv \frac{I_{\tau a} t_0}{C_t}$ $Z \equiv \frac{cI_{d\_tail}}{I_{bias} C_t}(x-1)I_b t_0$,

and

$$Y - |Z| = \frac{I_{\tau a} t_0}{C_t} - \frac{cI_{d\_tail} I_b t_0}{I_{bias} C_t}|x-1| = \frac{cI_{d\_tail} \cdot 2I_b t_0}{I_{bias} C_t} - \frac{cI_{d\_tail} I_b t_0}{I_{bias} C_t}|x-1| = \frac{cI_{d\_tail} I_b t_0}{I_{bias} C_t}(2 - |x-1|) > 0$$

For the purpose of comparison between actual and ideal case offsets, the adaptation time t_0 can be taken to be fixed, then X, Y and Z are constants which do not change with time.

Thus we have derived the condition on I_{ny1} required to balance the current mirror mismatch $1:x$. We now investigate the mismatch tuning for different assumptions about the current mirror ratio x.

In the case of a 1:1 current mirror ratio, $V_{c\_\tau}(desired) = \frac{1}{C_\tau}\int_0^{t_0}(I_1 - I_2)dt$, which is the desired voltage value that causes V_{τ_est} to track V_τ. In the case of a $1:x$ current mirror, $V_{c\_\tau}(real) = \frac{1}{C_\tau}\int_0^{t_0}\left(I_1' - xI_2'\right)dt$, which is the real voltage including the effect of offset current I_{ny1}. When $I_{ny1} = X \cdot \frac{Y - V_{c\_\tau}}{Z + V_{c\_\tau}}$, the real voltage is equal to the desired voltage,

which compensates the current mirror mismatch accurately so that V_{τ_est} tracks V_τ very well.

Condition 1): $x = 1 \Rightarrow I_{ny1} = 0$ as we expect.

Condition 2): $x > 1 \Rightarrow X > 0$, $Y > 0$, and $Z > 0$.

In the above development, we have derived the value for I_{ny1} which allows it to exactly cancel a current mirror mismatch. However, x is unknown, and I_{ny1} is an input to the circuit so it is likely that under some circumstances the value will not be correct for cancellation. We now examine the consequences of values for I_{ny1} which do not provide such cancellation.

Since $I_{ny1} > 0$, we know that $-Z < V_{c\_\tau} < Y$, so $\left(Z + V_{c\_\tau}\right) > 0$.

Let us go back to equations (2.41) to (2.45).

$$I_{ny1} > X \cdot \frac{Y - V_{c\_\tau}}{Z + V_{c\_\tau}} \Rightarrow \int_0^{t_0} (I_1 - I_2)dt < \int_0^{t_0} \left(I_1{}' - xI_2{}' \right) dt \Rightarrow V_{c\_\tau}(desired) < V_{c\_\tau}(real)$$
$$\Rightarrow V_\tau = V_{\tau\_est}(desired) > V_{\tau\_est}(real)$$

When the current I_{ny1} is larger than the compensating value $X \cdot \frac{Y - V_{c\_\tau}}{Z + V_{c\_\tau}}$, the time constant control voltage V_{τ_est} will be lower than the desired value V_τ.

$$I_{ny1} < X \cdot \frac{Y - V_{c\_\tau}}{Z + V_{c\_\tau}} \Rightarrow \int_0^{t_0} (I_1 - I_2)dt > \int_0^{t_0} \left(I_1{}' - xI_2{}' \right) dt \Rightarrow V_{c\_\tau}(desired) > V_{c\_\tau}(real)$$
$$\Rightarrow V_\tau = V_{\tau\_est}(desired) < V_{\tau\_est}(real)$$

When the current I_{ny1} is smaller than the compensating value $X \cdot \frac{Y - V_{c\_\tau}}{Z + V_{c\_\tau}}$, the time constant control voltage V_{τ_est} will be higher than the desired value V_τ.

These tuning relationships between I_{ny1} and V_{τ_est} have been observed in the experimental results of chip No.7.

Next we consider the effect of the gain change on the time constant adaptation. In Figure 2.12 and Figure 2.13 we observe that the gain adaptation affects the estimated the time constant control voltage. In the adaptation process shown in Figure 2.12 and Figure 2.13, I_{ny1} does not change. If the DC bias of the input signal to both plant and model filters does not change, the DC bias I_b of the output currents I_p and I_f will increase as the gain increases, and will decrease as the gain decreases. Recall that the gain of the lowpass filter topology can be expressed as $e^{K(V_{gain}-V_{g\_ref})}$, so the gain will increase as V_{gain} increases, and will decrease as V_{gain} decreases.

Assume that V_{τ_est} tracks V_τ accurately and has converged to V_τ, which implies

$$I_{ny1} = X \cdot \frac{Y - V_{c\_\tau}}{Z + V_{c\_\tau}} \Rightarrow V_{c\_\tau} = \frac{XY - ZI_{ny1}}{X + I_{ny1}} \Rightarrow \frac{\partial V_{c\_\tau}}{\partial Z} = -\frac{I_{ny1}}{X + I_{ny1}}.$$

Recall that X and I_{ny1} are positive, thus $\dot{V}_{c\_\tau}$ and $\dot{Z}$ are opposite in sign, so V_{c_τ} and Z change in opposite directions.

$$V_{gain} \uparrow \Rightarrow gain \uparrow \Rightarrow I_b \uparrow \Rightarrow Z \equiv \frac{cI_{d\_tail}}{I_{bias}C_t}(x-1)I_b t_0 \uparrow \text{ when } x > 1.$$

When the trimming current I_{ny1} does not change, V_{c_τ} must decrease to compensate the increase in Z, then $V_{c\_\tau} \downarrow \Rightarrow V_{\tau\_est} \uparrow$, which pushes V_{τ_est} higher as shown in Figure 2.12 at the time marked by the symbol *.

$$V_{gain} \downarrow \Rightarrow gain \downarrow \Rightarrow I_b \downarrow \Rightarrow Z \equiv \frac{cI_{d\_tail}}{I_{bias}C_t}(x-1)I_b t_0 \downarrow \text{ when } x > 1.$$

When the trimming current I_{ny1} does not change, V_{c_τ} must increase to compensate the decrease in Z, then $V_{c\_\tau} \uparrow \Rightarrow V_{\tau\_est} \downarrow$, which drags V_{τ_est} lower as shown in Figure 2.12 at the time marked by the symbol **.

Finally, we consider the effect of the time constant change on the time constant adaptation. What happens if the time constant control voltage V_τ of the plant changes? Should I_{ny1} also change to accurately compensate the current mirror mismatch? Here we investigate this problem by differentiating equation (2.45). Assuming that the gain does not change, then X, Y and Z are all constants which gives $\dot{X} = \dot{Y} = \dot{Z} = 0$

$$\dot{I}_{ny1} = X \frac{-\dot{V}_{c\_\tau}(Z + V_{c\_\tau}) - \dot{V}_{c\_\tau}(Y - V_{c\_\tau})}{(Z + V_{c\_\tau})^2} = \frac{-X(Y+Z)}{(Z + V_{c\_\tau})^2} \dot{V}_{c\_\tau}$$

$$\frac{\partial I_{ny1}}{\partial V_{c\_\tau}} = \frac{-X(Y+Z)}{(Z + V_{c\_\tau})^2} \qquad (2.46)$$

Recall that X, Y and Z are all positive, thus $\dot{I}_{ny1}$ and $\dot{V}_{c\_\tau}$ are opposite in sign, so I_{ny1} and V_{c_τ} change in opposite directions.

If V_τ increases, then in order for V_{τ_est} to track the change, V_{c_τ} must decrease, which implies that I_{ny1} must increase.

If V_τ decreases, then in order for V_{τ_est} to track the change, V_{c_τ} must increase, which implies that I_{ny1} must decrease.

This tuning relationship between I_{ny1} and V_τ has been observed in the experimental results of chip No.7.

Condition 3): $0 < x < 1 \Rightarrow X < 0$, $Y > 0$, and $Z < 0$

We now examine the consequences of values for I_{ny1} which do not provide the exact mismatch cancellation in the case of $0 < x < 1$.

Since $I_{ny1} > 0$, we know that either $V_{c\_\tau} < -Z$ or $V_{c\_\tau} > Y$

From equation (2.6), $(Y - V_{c\_\tau})$ was originally derived from $\frac{c}{I_{bias} C_t} \int_0^{t_0} I_2 dt$, which is strictly positive. Thus we conclude that $Y > V_{c\_\tau}$ and $V_{c\_\tau} < -Z$, so $V_{c\_\tau} + Z < 0$.

Let us go back to equations (2.41) to (2.45).

$$I_{ny1} > X \cdot \frac{Y - V_{c\_\tau}}{Z + V_{c\_\tau}} \Rightarrow \int_0^{t_0} (I_1 - I_2) dt > \int_0^{t_0} \left(I_1' - x I_2' \right) dt \Rightarrow V_{c\_\tau}(desired) > V_{c\_\tau}(real)$$
$$\Rightarrow V_\tau = V_{\tau\_est}(desired) < V_{\tau\_est}(real)$$

When the current I_{ny1} is larger than the compensating value $X \cdot \frac{Y - V_{c\_\tau}}{Z + V_{c\_\tau}}$, the time constant control voltage V_{τ_est} will be higher than the desired value V_τ.

$$I_{ny1} < X \cdot \frac{Y - V_{c\_\tau}}{Z + V_{c\_\tau}} \Rightarrow \int_0^{t_0} (I_1 - I_2) dt < \int_0^{t_0} \left(I_1' - x I_2' \right) dt \Rightarrow V_{c\_\tau}(desired) < V_{c\_\tau}(real)$$
$$\Rightarrow V_\tau = V_{\tau\_est}(desired) > V_{\tau\_est}(real)$$

When the current I_{ny1} is smaller than the compensating value $X \cdot \frac{Y - V_{c\_\tau}}{Z + V_{c\_\tau}}$, the time constant control voltage V_{τ_est} will be lower than the desired value V_τ.

These tuning relationships between I_{ny1} and V_{τ_est} have been observed in the experimental results of chip No.9.

Next, the effect of the gain change on the time constant adaptation is considered.

Assume that V_{τ_est} tracks V_τ accurately and has converged to V_τ, which implies

$$I_{ny1} = X \cdot \frac{Y - V_{c\_\tau}}{Z + V_{c\_\tau}} \Rightarrow V_{c\_\tau} = \frac{XY - ZI_{ny1}}{X + I_{ny1}} \Rightarrow \frac{\partial V_{c\_\tau}}{\partial Z} = -\frac{I_{ny1}}{X + I_{ny1}}.$$

Recall that X and Z are negative, and $V_{c\_\tau} + Z < 0 \Rightarrow V_{c\_\tau} - |Z| < 0 \Rightarrow |Z| - V_{c\_\tau} > 0$.

Recall that $Y - |Z| > 0 \Rightarrow Y - V_{c\_\tau} > |Z| - V_{c\_\tau} \Rightarrow \frac{Y - V_{c\_\tau}}{|Z| - V_{c\_\tau}} = \frac{I_{ny1}}{-X} > 1 \Rightarrow I_{ny1} + X > 0$. Since I_{ny1} is also positive, $\dot{V}_{c\_\tau}$ and $\dot{Z}$ are opposite in sign, so V_{c_τ} and Z change in opposite directions.

$$V_{gain} \uparrow \Rightarrow gain \uparrow \Rightarrow I_b \uparrow \Rightarrow Z \equiv \frac{cI_{d\_tail}}{I_{bias}C_t}(x-1)I_b t_0 \downarrow \text{ when } 0 < x < 1.$$

When the trimming current I_{ny1} does not change, V_{c_τ} must increase to compensate the decrease in Z, then $V_{c\_\tau} \uparrow \Rightarrow V_{\tau\_est} \downarrow$, which drags V_{τ_est} lower as shown in Figure 2.13 at the time marked by the symbol #.

$$V_{gain} \downarrow \Rightarrow gain \downarrow \Rightarrow I_b \downarrow \Rightarrow Z \equiv \frac{cI_{d\_tail}}{I_{bias}C_t}(x-1)I_b t_0 \uparrow \text{ when } 0 < x < 1.$$

When the trimming current I_{ny1} does not change, V_{c_τ} must decrease to compensate the decrease in Z, then $V_{c\_\tau} \downarrow \Rightarrow V_{\tau\_est} \uparrow$, which pushes V_{τ_est} higher as shown in Figure 2.13 at the time marked by the symbol ##.

Finally, we consider the effect of the time constant change on the time constant adaptation. Again we investigate this problem by differentiating equation (2.7). Assuming that the gain does not change, then X, Y and Z are all constants which gives $\dot{X} = \dot{Y} = \dot{Z} = 0$.

$$\dot{I}_{ny1} = X \frac{-\dot{V}_{c\_\tau}(Z + V_{c\_\tau}) - \dot{V}_{c\_\tau}(Y - V_{c\_\tau})}{(Z + V_{c\_\tau})^2} = \frac{-X(Y+Z)}{(Z + V_{c\_\tau})^2}\dot{V}_{c\_\tau}$$

$$\frac{\partial I_{ny1}}{\partial V_{c\_\tau}} = \frac{-X(Y+Z)}{(Z+V_{c\_\tau})^2} \qquad (2.46)$$

Recall that X and Z are negative, and $Y-|Z|=Y+Z>0$, thus $\dot{I}_{ny1}$ and $\dot{V}_{c\_\tau}$ have the same sign, so I_{ny1} and V_{c_τ} change in the same directions.

If V_τ increases, then in order for V_{τ_est} to track the change, V_{c_τ} must increase, which implies that I_{ny1} must decrease.

If V_τ decreases, then in order for V_{τ_est} to track the change, V_{c_τ} must decrease, which implies that I_{ny1} must increase.

These tuning relationships between I_{ny1} and V_τ have been observed in the experimental results of chip No.9

Table 2.1 summarizes the results of the mismatch analysis. In this table, $I_{comp} \equiv X \cdot \frac{Y-V_{c\_\tau}}{Z+V_{c\_\tau}}$.

	I_{ny1} vs I_{comp}	$gain$ vs V_{t_est}	V_τ vs I_{comp}
$x>1$	$I_{ny1}>I_{comp} \Rightarrow V_{\tau\_est}<V_\tau$	$gain\uparrow \Rightarrow V_{\tau\_est}\uparrow$ *	$V_\tau\uparrow \Rightarrow I_{comp}\uparrow$
	$I_{ny1}<I_{comp} \Rightarrow V_{\tau\_est}>V_\tau$	$gain\downarrow \Rightarrow V_{\tau\_est}\downarrow$ **	$V_\tau\downarrow \Rightarrow I_{comp}\downarrow$
$0<x<1$	$I_{ny1}>I_{comp} \Rightarrow V_{\tau\_est}>V_\tau$	$gain\uparrow \Rightarrow V_{\tau\_est}\downarrow$ #	$V_\tau\uparrow \Rightarrow I_{comp}\downarrow$
	$I_{ny1}<I_{comp} \Rightarrow V_{\tau\_est}<V_\tau$	$gain\downarrow \Rightarrow V_{\tau\_est}\uparrow$ ##	$V_\tau\downarrow \Rightarrow I_{comp}\uparrow$

Table 2.1: Results of the mismatch analysis.

2.6 Summary

We have described adaptive first order lowpass filters implemented using a log domain architecture and MITE circuits, along with MITE circuits which integrate the learning rules for system identification. We chose to implement adaptive filters using a log domain topology because log domain filters are compact current mode IIR filters that operate with low power, have wide tuning range, large dynamic range, and capability for high frequency operation. Further, we've developed robust learning rules based on Lyapunov stability. These learning rules are implemented using MITE structures, highlighting the elegance and symbiotic nature of the design methodology.

Experimental results of the 0.5μm CMOS chip show stable adaptation under a variety of conditions, which demonstrates the success of our adaptive system design using this model-based learning method.

Chapter 3: Adaptation of Second Order Filters

Adaptive log domain first order lowpass filters have been considered in Chapter 2. The adaptation of second order filters is discussed in this chapter.

The design of the second order filter [16] is presented in section 3.1. Learning rules for the second order filters [17] are derived in section 3.2 based on Lyapunov methods. MITE implementations of the learning rules are discussed in section 3.3. The derivative circuit and the four quadrant multiplication circuit discussed in Chapter 2 are used to implement the learning rules for the parameters, quality factor and time constant of the second order filter. Simulation results with HSPICE using BSIM3v3 models for a 0.5μm technology are shown in section 3.4. The quality factor and time constant parameters accurately and stably track the quality factor and time constant of the plant filter, and the output difference between the estimated filter and the plant filter approaches zero when adaptation is complete.

3.1 Second Order Filter Design

We synthesize higher-order log domain filters by factoring the desired transfer function into first order equations which are simple to implement. We illustrate the method by designing a second order bandpass filter.

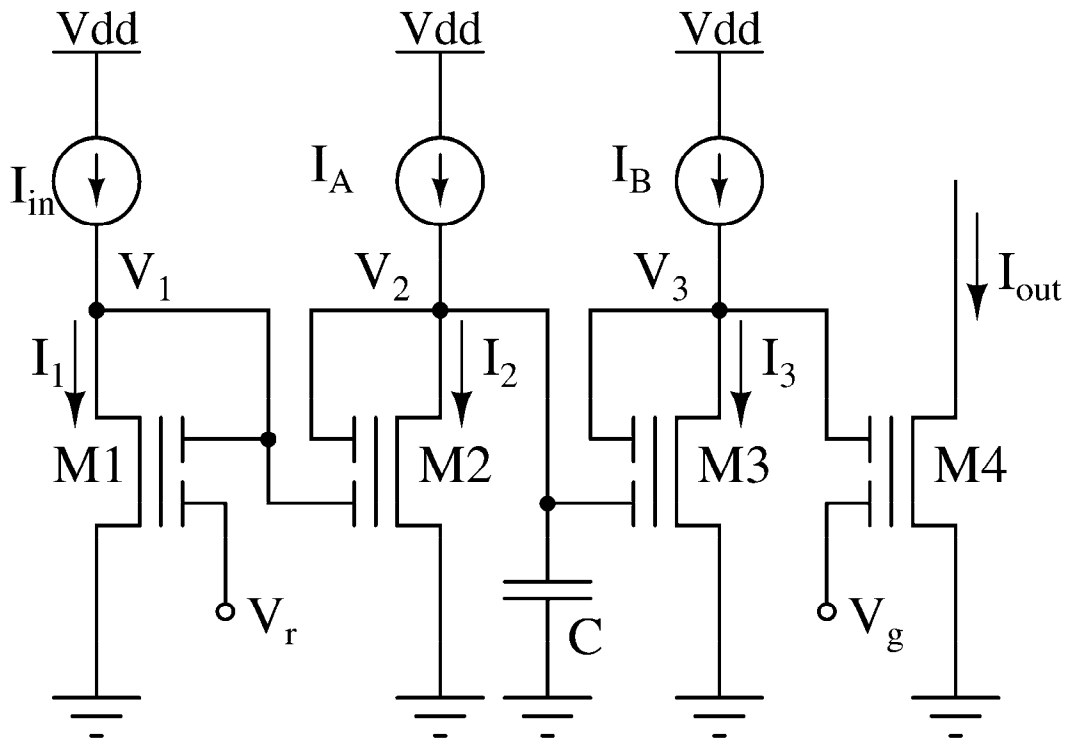

Figure 3.1: MITE implementation for first order lowpass filter

3.1.1 First Order Lowpass filter structure

Figure 3.1 shows a first order lowpass filter structure implemented using multiple input floating gate transistors. Suppose that the input voltages of the floating gate transistors are equally weighted. In subthreshold operation FGMOS current is an exponential function of the summed inputs:

$$I_1 = I_0 e^{\kappa(V_1+V_r)/2U_T} = I_{in} \tag{3.1}$$

$$I_2 = I_0 e^{\kappa(V_1+V_2)/2U_T} \tag{3.2}$$

$$I_3 = I_0 e^{\kappa(V_2+V_3)/2U_T} = I_B \tag{3.3}$$

$$I_4 = I_0 e^{\kappa(V_3+V_g)/2U_T} = I_{out} \tag{3.4}$$

We apply Kirchoff's Current Law (KCL) at the capacitive node to find relationship between the MITE currents and the capacitive current:

$$C\dot{V}_2 + I_2 = I_A = C\dot{V}_2 + \frac{I_{in}I_B}{I_{out}} e^{\kappa(V_g-V_r)/2U_T} \tag{3.5}$$

Since V_2 and V_3 together control a constant current I_3, their time derivatives are opposite in sign but equal in magnitude:

$$\dot{I}_3 = I_3 \cdot \frac{\kappa}{2U_T}\left(\dot{V}_2 + \dot{V}_3\right) = 0 \Rightarrow \dot{V}_3 = -\dot{V}_2 \tag{3.6}$$

We determine the output current I_{out} by differentiating it.

$$\begin{aligned} &\dot{I}_{out} = I_{out}\frac{\kappa}{2U_T}\dot{V}_3 = -I_{out}\frac{\kappa}{2U_T}\dot{V}_2 \\ &\Rightarrow \dot{I}_{out} = -I_{out}\frac{\kappa}{2U_T C}\left[I_A - \frac{I_{in}I_B}{I_{out}} e^{\kappa(V_g-V_r)/2U_T}\right] \\ &\Rightarrow \frac{I_{out}}{I_{in}} = \frac{e^{\kappa(V_g-V_r)/2U_T}}{\left(I_A/I_B\right)+\left(2U_T C/\kappa I_B\right)s} \end{aligned} \tag{3.7}$$

If $I_A = I_B$, we obtain a first order lowpass transfer function with time constant $2U_T C / \kappa I_B$ and gain $e^{\kappa(V_g - V_r)/2U_T}$.

3.1.2 Second Order Bandpass Filter structure

We synthesize higher-order log domain filters by factoring the desired transfer function into first order equations [18] which can be directly implemented using the simple block shown in Figure 3.1. We illustrate the method by designing a second order bandpass filter. We first specify the desired bandpass transfer function:

$$\frac{I_{out}}{I_{in}} = \frac{g \cdot \tau \cdot s}{1 + (1/Q) \cdot \tau \cdot s + \tau^2 \cdot s^2} \qquad (3.8)$$

This describes a bandpass filter with gain of g, quality factor of Q and time constant of τ. Note that the bandpass function eliminates DC components of the input signal, whereas currents in log domain filters are positive. An output bias must be added to ensure that MITE currents are strictly positive.

For simplicity of implementation, we add a DC current term divided by the denominator of the bandpass transfer function. The filter performs a second-order low pass filtering operation on the DC component, which does not affect the output bias at low frequencies. To further simplify the implementation, we synthesize the second order filter without gain and incorporate it later.

$$I_{out} = \frac{g \cdot (\tau \cdot s \cdot I_{in} + I_{DC})}{1 + (1/Q) \cdot \tau \cdot s + \tau^2 \cdot s^2} \qquad (3.9)$$

We consider intermediate currents I_x and I'_{out},

$$I'_{out} = I_{out} / g \qquad (3.10)$$

$$I_x = \frac{I_{in} - (1/Q + \tau \cdot s) I_{DC}}{1 + (1/Q) \cdot \tau \cdot s + \tau^2 \cdot s^2} \tag{3.11}$$

The above function can be easily factored into two simple first order lowpass transfer functions:

$$\frac{I'_{out}}{I_{in} - I_x} = \frac{1}{1/Q + \tau \cdot s} \tag{3.12}$$

$$\frac{I_x}{I'_{out} - I_{DC}} = \frac{1}{\tau \cdot s} \tag{3.13}$$

In order to implement these two transfer functions using the structure in section 3.1.1, we need to ensure that the input signal remains positive. Since the numerators of both functions are unity, we do not need to consider the difference between V_r and V_g in Figure 3.1 and simply connect them together.

To implement equation (3.12), a straightforward adaptation of the lowpass structure is shown in Figure 3.2(a), where we take $I_A = I_B/Q$ and the time constant is $\tau = 2U_T C/\kappa I_B$. However, the first order filter structure requires the input signal to be positive, and I_{in}-I_x can be negative. A solution to this problem is shown in the equivalent circuit of Figure 3.2(b). The translinear loop equations for Figure 3.2(a) and (b) can be written as:

$$(I_{in} - I_x) I_B = (I_B / Q - I_C) I'_{out} \tag{3.14}$$

$$I_{in} I_B = (I_B / Q + I'_x - I_C) I'_{out} \tag{3.15}$$

If we set the dependent current source to be $I'_x = I_x I_B / I'_{out}$, equations (3.14) and (3.15) are equivalent. Thus we introduce a dependent current source at the capacitive node in order to resolve the potential problem of negative inputs. We can implement equation (3.13) using the same method, with the resulting circuits shown in Figure 3.3. Here the

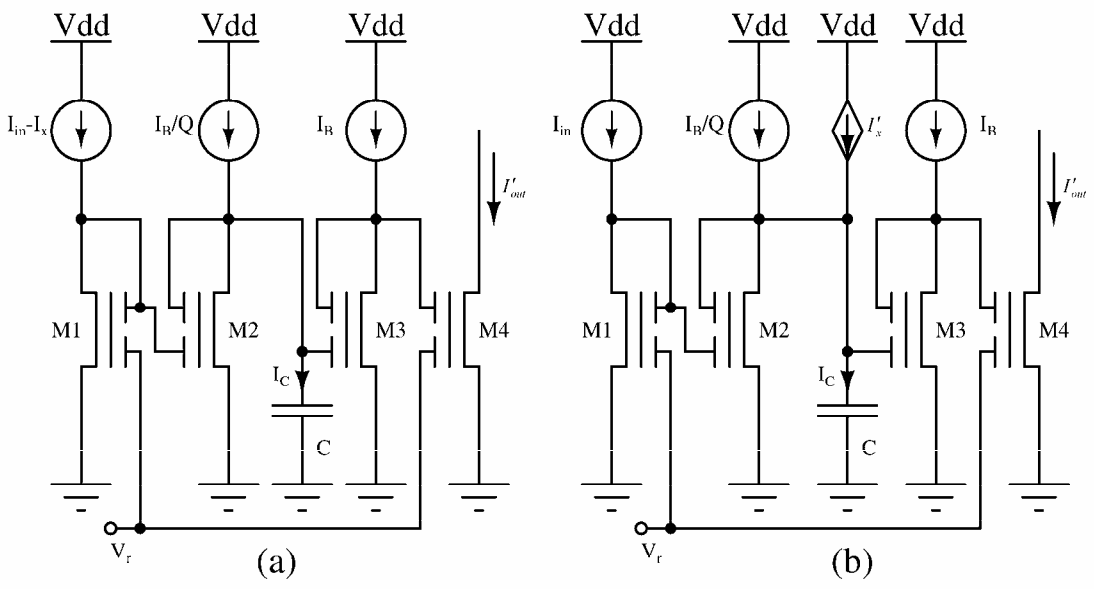

Figure 3.2: Circuit for implementing Equation (3.12): (a) a straightforward idea which is unrealizable; (b) equivalent implementation.

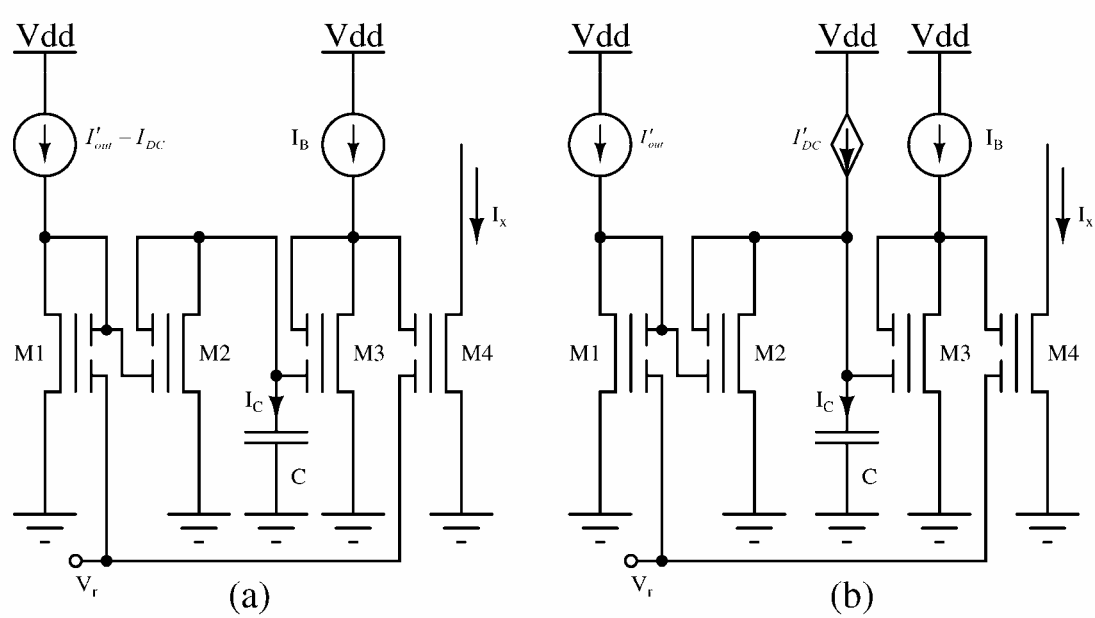

Figure 3.3: Circuit for implementing Equation (3.13): (a) a straightforward idea which is unrealizable; (b) equivalent implementation.

dependent source is $I'_{DC}=I_{DC}I_B/I_x$.

We cascade the circuits in Figure 3.2(b) and Figure 3.3(b) to realize the second order transfer function for I'_{out} as shown in Figure 3.4. The final issue is implementation of the two dependent current sources I'_x and I'_{DC}.

MITE transistors M4, M5, M6 and M7 form a translinear loop which gives an elegant expression: $I'_{out}I_B=I_yI_x$. Using this expression, the dependent current sources can be written as:

$$I'_x = I_x I_B / I'_{out} = I_B^2 / I_y \tag{3.16}$$

$$I'_{DC} = I_{DC} I_B / I_x = I_{DC} I_y / I'_{out} \tag{3.17}$$

Thus, both dependent current sources are expressed in terms of I_y instead of I_x, and transistors M6 and M7 inside the dotted box in Figure 3.4 which generate I_x are not necessary. The two dependent current sources are implemented using translinear loops as shown in Figure 3.5. MITE transistors M4, M5, M8 and M9 form a translinear loop to realize $I'_{DC}=I_{DC}I_y/I'_{out}$, which is sourced into the second capacitive node. MITE transistors M6, M7, M5 and M3 form another translinear loop to implement $I'_x=I_B^2/I_y$, which is sourced into the first capacitive node. Thus we complete the realization of the dependent current sources. The quality factor Q is implemented by using V_Q rather than Vdd as the source voltage for PMOS transistor M11. Since all the transistors are working in subthreshold, current can be expressed as the exponential of the control voltage. Neglecting the body effect, we have

$$I_B / Q = I_0 e^{(V_Q - V_B - |V_{thp}|)/U_T} \tag{3.18}$$

$$I_B = I_0 e^{(V_{dd} - V_B - |V_{thp}|)/U_T} \tag{3.19}$$

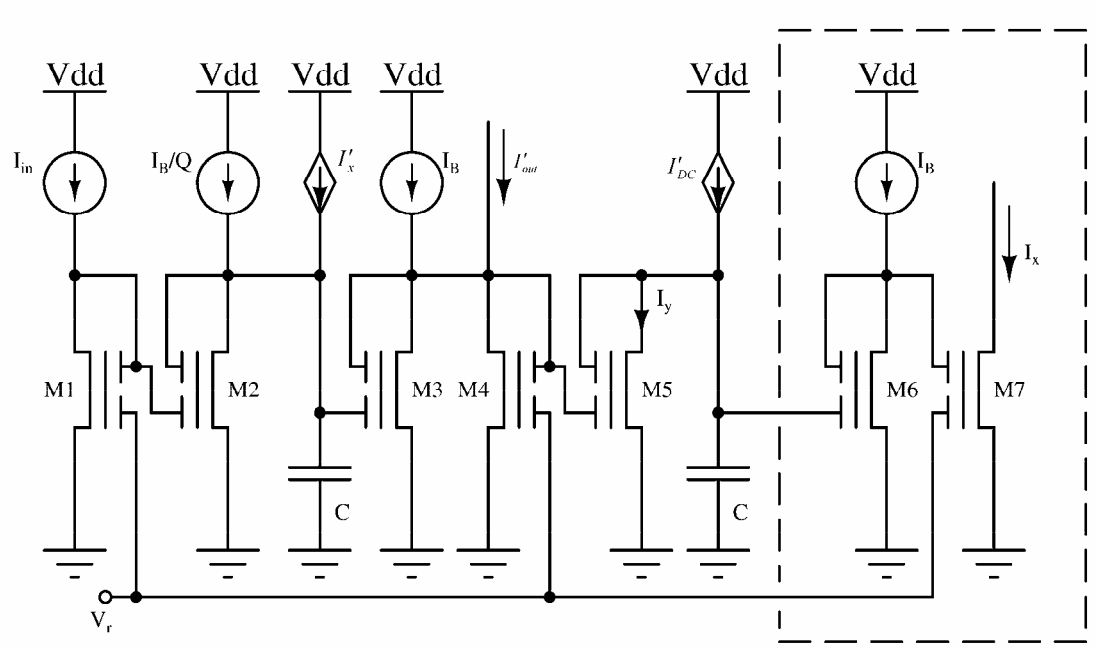

Figure 3.4: Circuit for second order filter with dependent current sources**.**

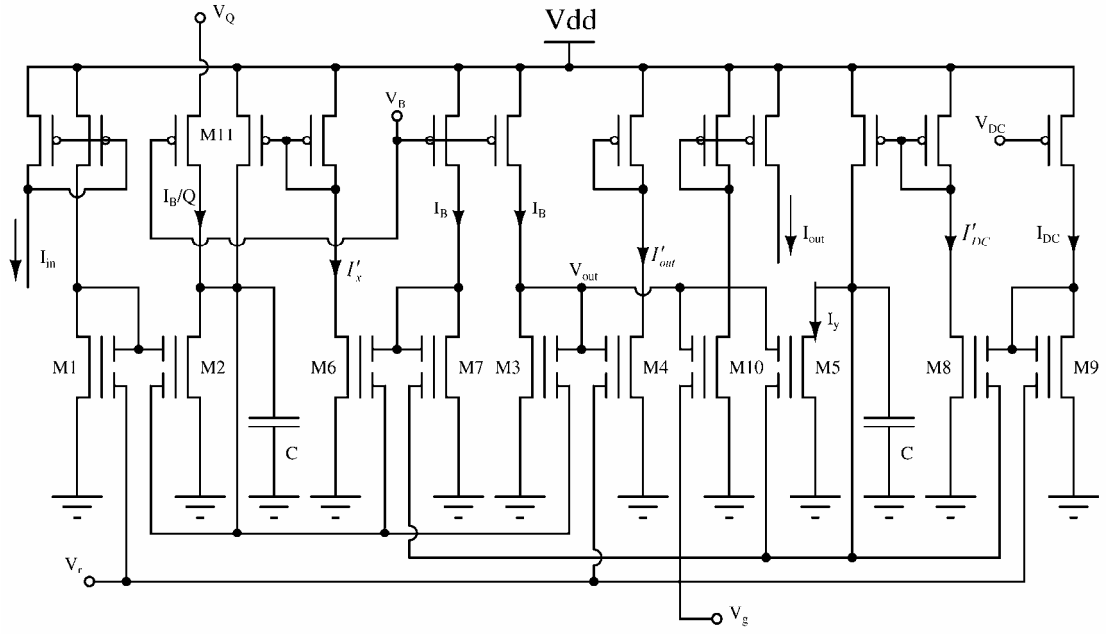

Figure 3.5: Complete circuit for the second order filter.

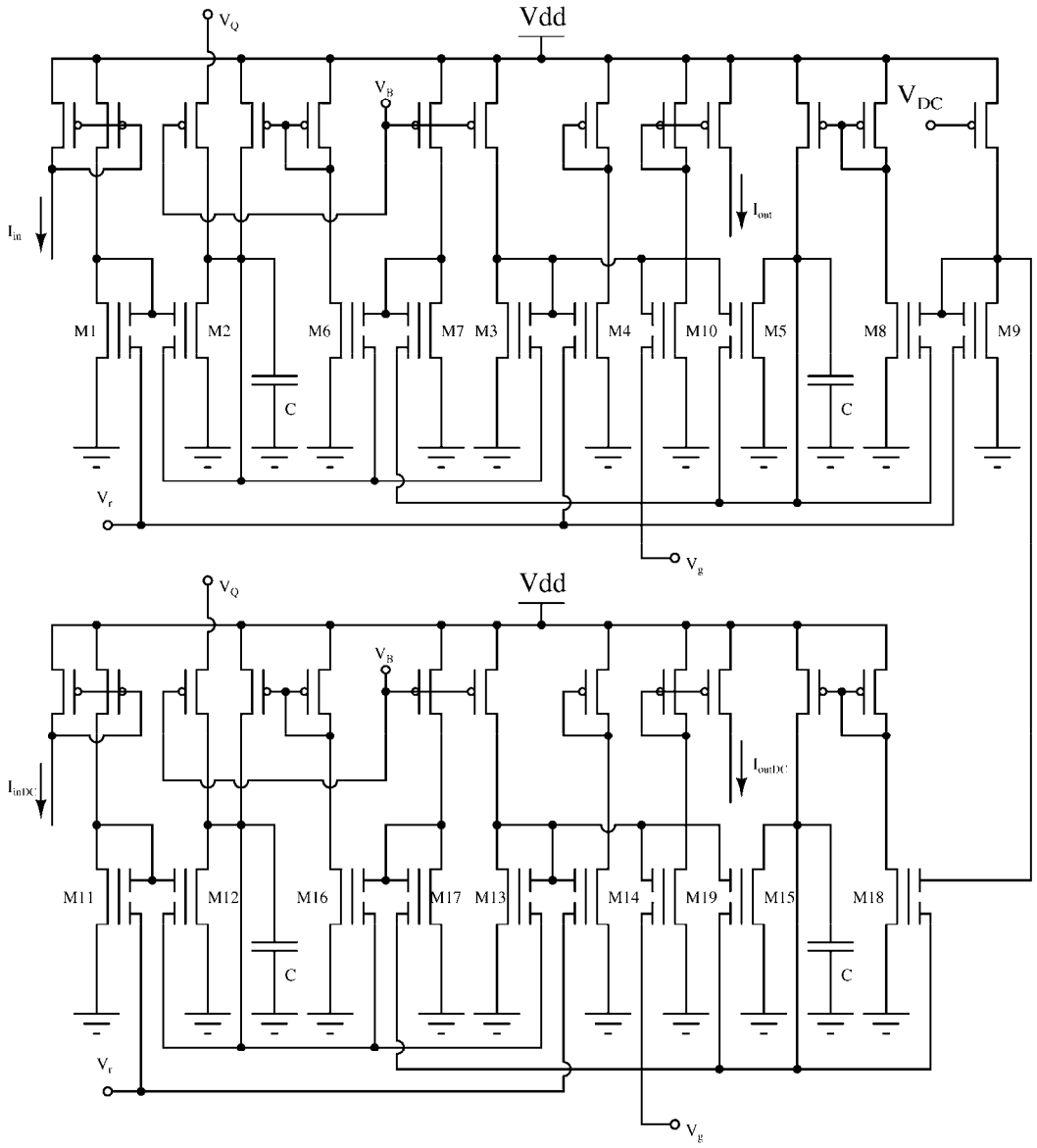

Figure 3.6: Complete circuit for the second order bandpass filter.

So the quality factor Q can be expressed as:

$$Q = e^{(V_{dd} - V_Q)/U_T} \tag{3.20}$$

M10 shares the input voltage V_{out} with M4, and has a different input voltage V_g, which implements the gain $g = e^{\kappa(V_g - V_r)/2U_T}$ and produces the final output current I_{out}=gI'_{out}. This output current exhibits the second order transfer characteristic:

$$I_{out} = \frac{g \cdot (\tau \cdot s \cdot I_{in} + I_{DC})}{1 + (1/Q) \cdot \tau \cdot s + \tau^2 \cdot s^2} \tag{3.9}$$

In order to implement a truly *bandpass* characteristic we use a similar structure M11-M19 shown in Figure 3.6 which shares the same constant current biases and removes the DC bias of the output. The output current is obtained by taking the difference $(I_{out} - I_{outDC})$ between the outputs of two similar structures. One is driven by the positive input signal I_{in} and the other is driven by the DC bias I_{inDC} of the input signal I_{in}.

3.1.3 Simulation Results

We simulate the circuit with HSPICE using BSIM3v3 models for a 0.5μm commercially available technology. The technique in [14] is used to avoid floating-node problems in the simulator. The filter is powered using a voltage supply of 1.5V and the bias of the output current is set at 100nA. We initialize all the floating gate nodes and drain nodes of the transistors to half of the power supply (0.75V) to ensure to maximum operating range and accuracy of simulation. Transient simulation results of a sinusoidal input signal show that the output of the filter does not vary sinusoidally initially, but as the internal node voltages equilibrate, it eventually behaves as expected. The initial time

required for startup may be minimized if we can tune the initial voltage of every node in the circuit perfectly. But for different time constant currents or different quality factor control voltages, the perfectly-tuned initial voltage of every node varies from one condition to another. Thus it is not safe to use AC simulation to determine the transfer function under those different initial conditions. Instead, we simulate the filter transiently at different frequencies, and plot all the output current amplitudes with respect to the frequencies for each condition.

First we sweep the time constant current I_B linearly from 20nA to 60nA. The central frequency is proportional to the reciprocal of the time constant, and the current I_B is proportional to the reciprocal of the time constant. So the central frequency varies linearly with the current I_B as shown in Figure 3.7. For these simulations, V_r=V_{gain}=0.75V, and V_Q=1.45V.

Next we sweep the quality factor Q by varying the voltage V_Q from 1.43V to 1.47V linearly. According to equation (3.5) the quality factor Q is swept exponentially as shown in Figure 3.8. For these simulations, V_r=V_{gain}=0.75V, and I_B=40nA.

Finally we show the gain dependence on gain control voltage V_g. With the constant voltage V_r at 0.75V, we vary V_g linearly from 0.65V to 0.85V. The gain is proportional to the exponential of the voltage V_g. Figure 3.9 depicts the linearity of the gain (dB) change with the gain control voltage V_g. For these simulations, I_B=40nA and V_Q=1.45V. The input signal is a 10kHz sine wave.

From Figure 3.7, the operating point I_B=*40nA* corresponds to a central frequency around 20kHz, which gives the time constant as:

$$\tau = \frac{1}{2\pi f} = \frac{1}{2\pi \cdot 2\times 10^4} \qquad (3.21)$$

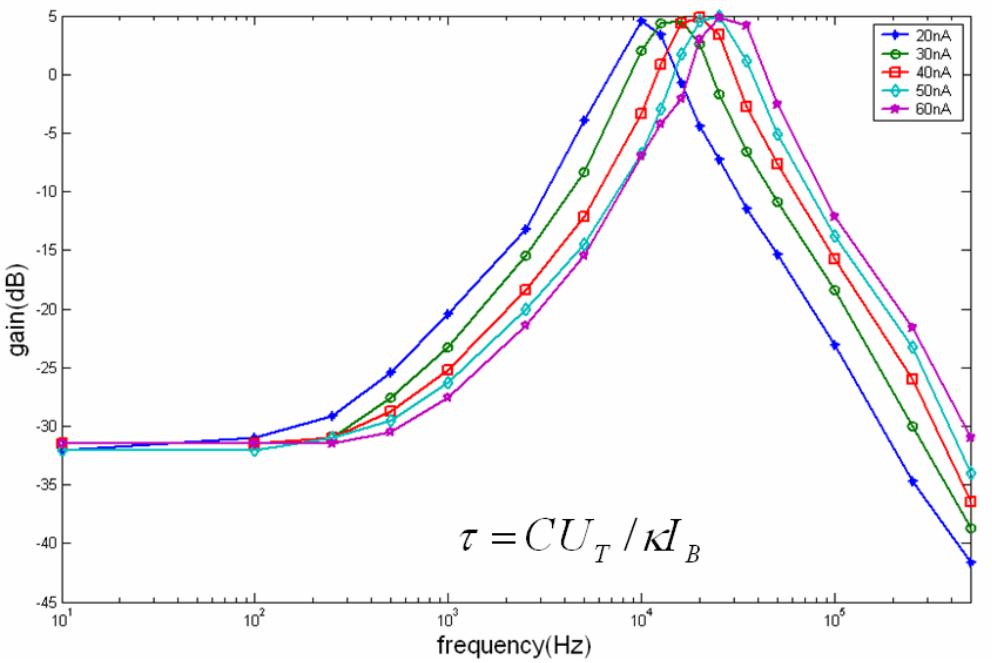

Figure 3.7: Time constant τ tuning with time constant current swept from 20nA to 60nA linearly with V_r=V_{gain}=0.75V and V_Q=1.45V

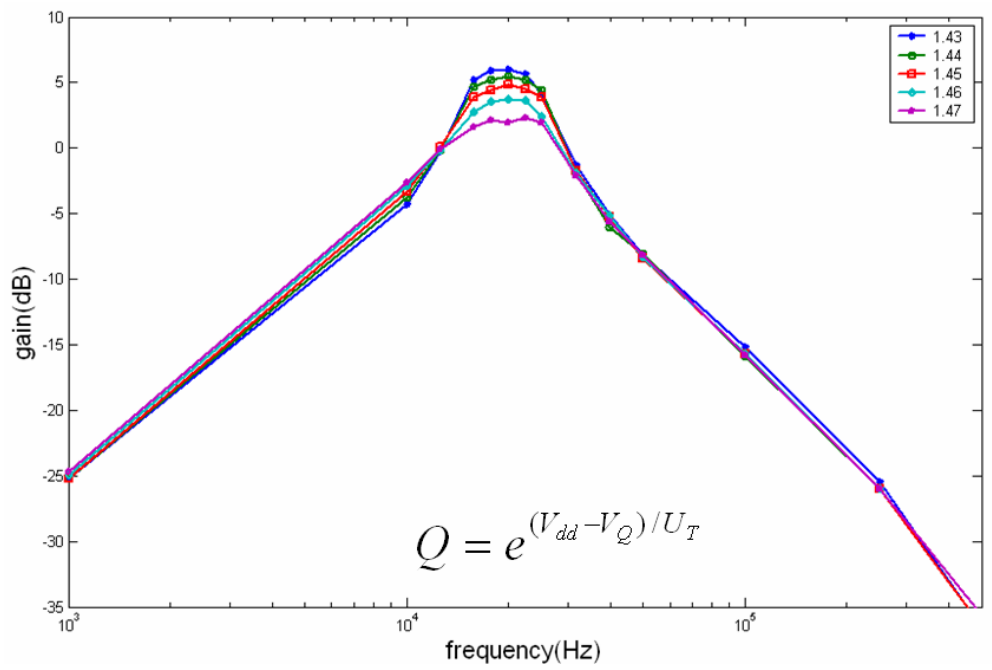

Figure 3.8: Quality factor Q tuning with voltage V_Q swept from 1.43V to 1.47V linearly with V_r=V_{gain}=0.75V and I_B=40nA.

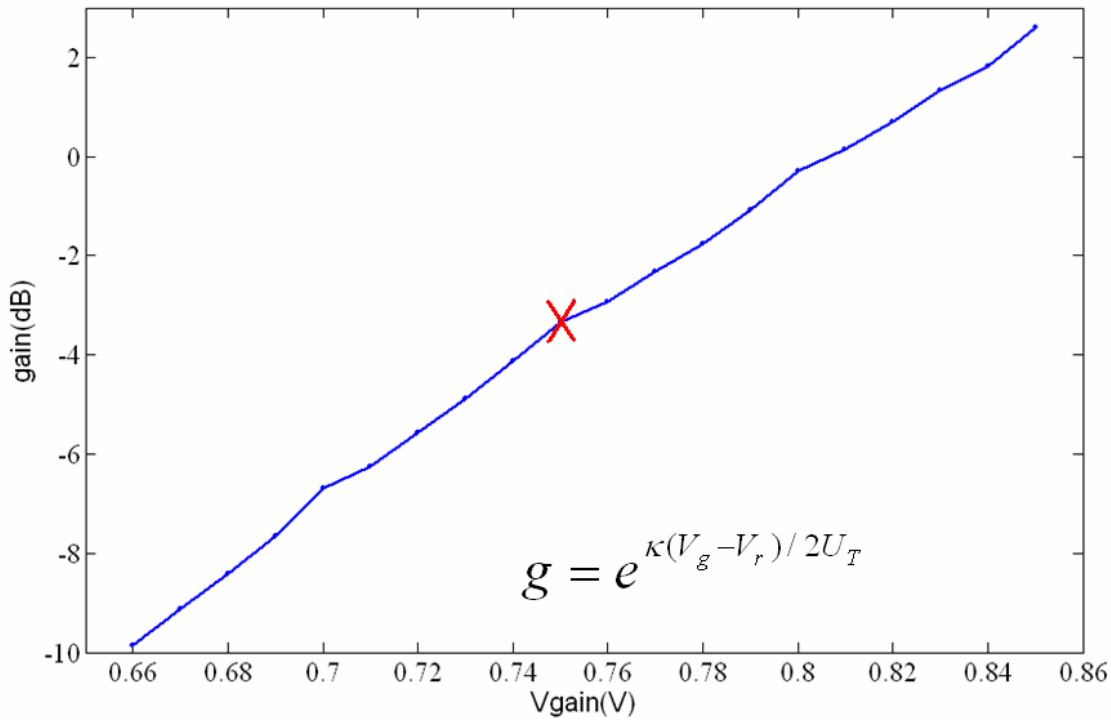

Figure 3.9: Gain dependence on gain control voltage V_g with I_B=40nA and V_Q=1.45V.

According to simulation results, $V_Q = 1.45V$ corresponds to $Q=4.31$. At a frequency of 10kHz with $V_g=0.75V$ which gives s as:

$$s = 2\pi f \cdot j = 2\pi \cdot 1\times 10^4 j \qquad (3.22)$$

so that

$$\tau \cdot s = \frac{1}{2\pi \cdot 2\times 10^4} \cdot 2\pi \cdot 1\times 10^4 j = 0.5j \qquad (3.23)$$

the gain can be calculated as

$$20\log_{10}\left|\frac{\tau \cdot s}{1+\tau \cdot s/Q+\tau^2 s^2}\right| = 20\log_{10}\left|\frac{0.5j}{1+0.5j/4.31+(0.5j)^2}\right| = -3.6dB \qquad (3.24)$$

which agrees well with the simulation result of *-3.3dB* in Figure 3.9 indicated by the symbol X.

3.2 Derivation of Learning Rules

We describe a second order adaptive filter which addresses the classical problem of system identification depicted in Figure 3.10. A tunable second order filter is used as the model to identify an unknown system. An input signal is applied to both an unknown system *(plant)* and an adaptive estimator *(model)* system. Control laws are designed using observable outputs to adjust the parameters of the estimator so as to ensure stability of the learning procedure.

The second order filter is described by the following equation:

$$I_{out}(s) = I_{in}(s) \cdot \frac{\tau \cdot s}{1+\frac{1}{Q}\cdot \tau \cdot s+\tau^2 \cdot s^2} + I_{DC} \cdot \frac{1}{1+\frac{1}{Q}\cdot \tau \cdot s+\tau^2 \cdot s^2} \qquad (3.25)$$

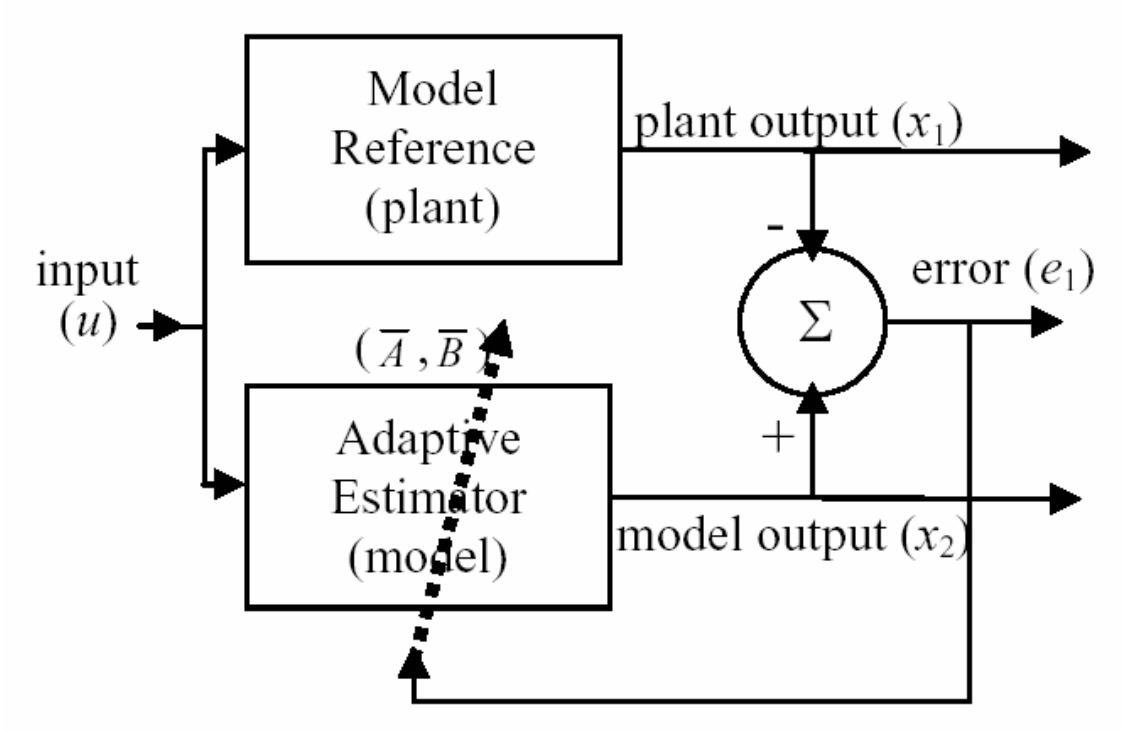

Figure 3.10: The system identification problem.

While the bandpass function eliminates DC components from the input, log domain filters are inherently current mode circuits with strictly positive currents. Thus we must introduce an output bias, denoted here as a constant current I_{DC}, which is independent of the input signal.

We describe the unknown plant and adaptive model filter using the state-variable representation:

$$\ddot{x}_1 = -B^2 x_1 - AB\dot{x}_1 + B\dot{u} + B^2 D \qquad \text{plant} \qquad (3.26)$$

$$\ddot{x}_2 = -\overline{B}^2 x_2 - \overline{A}\overline{B}\dot{x}_2 + \overline{B}\dot{u} + \overline{B}^2 D \qquad \text{model} \qquad (3.27)$$

where x_1 and x_2 are the plant and model outputs, A and $\overline{A}$ are the reciprocals of plant and model quality factors, B and $\overline{B}$ are the reciprocals of plant and model time constants, u is the input to both filters, and D is the output bias of both outputs.

An error system is constructed in order to evaluate the performance and stability of the adaptation.

$$e_1 = x_2 - x_1 \qquad \text{output error} \qquad (3.28)$$

$$e_2 = \overline{A} - A \qquad \text{(1/quality factor) error} \qquad (3.29)$$

$$e_3 = \overline{B} - B \qquad \text{(1/time constant) error} \qquad (3.30)$$

We seek control laws which drive all errors toward zero with time. Thus the dynamics of the error system should also be considered:

$$\dot{e}_1 = \dot{x}_2 - \dot{x}_1 \qquad (3.31)$$

$$\ddot{e}_1 = \ddot{x}_2 - \ddot{x}_1 \qquad (3.32)$$

$$\dot{e}_2 = \dot{\overline{A}} \qquad (3.33)$$

$$\dot{e}_3 = \dot{\overline{B}} \tag{3.34}$$

We cannot control the dynamics of the output error since that depends on the unknown input *u*, but we can derive adaptive laws that specify the dynamics of the parameter errors so that the estimator learns the behavior of unknown system.

The direct Lyapunov method is employed to derive appropriate learning rules [13]. We must find a scalar function which satisfies three conditions: positive definite, negative definite time derivative and radially unbounded. For the adaptation of the second order filter we consider the candidate Lyapunov function:

$$V(e) = \frac{1}{2}\left(\dot{e}_1^2 + B^2 e_1^2 + e_2^2 + e_3^2\right) \tag{3.35}$$

This function satisfies the first and third conditions. To evaluate the second condition, we evaluate the temporal derivative of the candidate function:

$$\dot{V}(e) = \dot{e}_1\ddot{e}_1 + B^2 e_1\dot{e}_1 + e_2\dot{e}_2 + e_3\dot{e}_3 \tag{3.36}$$

This temporal derivative is a function of the second derivative of the output difference, so we compute it as follows:

$$\begin{aligned}
\ddot{e}_1 = \ddot{x}_2 - \ddot{x}_1 &= \left(-\overline{B}^2 x_2 - \overline{A}\overline{B}\dot{x}_2 + \overline{B}\dot{u} + \overline{B}^2 D\right) - \left(-B^2 x_1 - AB\dot{x}_1 + B\dot{u} + B^2 D\right) \\
&= -\left(e_3 + B\right)^2 x_2 + B^2\left(x_2 - e_1\right) - \left(e_2 + A\right)\left(e_3 + B\right)\dot{x}_2 + AB\left(\dot{x}_2 - \dot{e}_1\right) + \overline{B}\dot{u} - B\dot{u} + \left(e_3^2 + 2e_3 B\right)D \\
&= -\left(e_3^2 + 2e_3 B\right)x_2 - B^2 e_1 - \left(e_2 e_3 + Ae_3 + Be_2\right)\dot{x}_2 - AB\dot{e}_1 + e_3\dot{u} + e_3\left(e_3 + 2B\right)D \\
&= -e_3\left(e_3 + 2B\right)x_2 - e_3\left(e_2 + A\right)\dot{x}_2 + e_3\dot{u} - Be_2\dot{x}_2 - B^2 e_1 - AB\dot{e}_1 + e_3\left(e_3 + 2B\right)D \\
&= e_3\left[\left(-\overline{B}x_2 - \overline{A}\dot{x}_2 + \dot{u} + \overline{B}D\right) - Bx_2 + BD\right] - Be_2\dot{x}_2 - B^2 e_1 - AB\dot{e}_1 \\
&= e_3\left[\frac{\ddot{x}_2}{\overline{B}} - B\left(x_2 - D\right)\right] - Be_2\dot{x}_2 - B^2 e_1 - AB\dot{e}_1
\end{aligned} \tag{3.37}$$

Next we substitute the expression for the second derivative into the temporal derivative of the candidate Lyapunov function:

$$\begin{aligned}\dot{V}(e) &= \dot{e}_1\ddot{e}_1 + B^2 e_1\dot{e}_1 + e_2\dot{e}_2 + e_3\dot{e}_3 \\ &= \dot{e}_1\left\{e_3\left[\frac{\ddot{x}_2}{\overline{B}} - B\left(x_2 - D\right)\right] - Be_2\dot{x}_2 - B^2 e_1 - AB\dot{e}_1\right\} + B^2 e_1\dot{e}_1 + e_2\dot{e}_2 + e_3\dot{e}_3 \\ &= -AB\dot{e}_1^2 + e_2\left(-B\dot{e}_1\dot{x}_2 + \dot{e}_2\right) + e_3\left\{\dot{e}_1\left[\frac{\ddot{x}_2}{\overline{B}} - B\left(x_2 - D\right)\right] + \dot{e}_3\right\}\end{aligned} \tag{3.38}$$

By choosing the following control laws:

$$\dot{e}_2 = B\dot{e}_1\dot{x}_2 \tag{3.39}$$

$$\dot{e}_3 = \dot{e}_1\left[B\left(x_2 - D\right) - \frac{\ddot{x}_2}{\overline{B}}\right] \tag{3.40}$$

we ensure that the candidate Lyapunov function has a negative time derivative:

$$\dot{V}\left(e\right) = -AB\dot{e}_1^2 \tag{3.41}$$

Assume that the output signal varies as a sinusoidal function $x_2 = D + E\sin\left(wt\right)$, where the frequency w is low and D is the output bias. We can express $\left(x_2 - D\right)$ and $\ddot{x}_2$ as follows:

$$x_2 - D = E\sin\left(wt\right) \tag{3.42}$$

$$\ddot{x}_2 = -Ew^2\sin\left(wt\right) \tag{3.43}$$

By substituting these expressions into the learning rule for the of time constant, we find that the update is the product of two signed quantities, $\dot{e}_1$ and $\left(x_2 - D\right)$, and a positive term $\left(B + \frac{w^2}{\overline{B}}\right)$ that depends on the signal frequency.

$$\dot{e}_3 = \dot{e}_1\left[BE\sin(wt) + \frac{Ew^2}{\overline{B}}\sin(wt)\right] = \dot{e}_1\left(B + \frac{w^2}{\overline{B}}\right)E\sin(wt)$$
$$= \dot{e}_1\left(B + \frac{w^2}{\overline{B}}\right)(x_2 - D)$$

(3.44)

The learning rule for time constant and quality factor may be simplified further since in current mode log domain filters the quality factors and time constants are positive. The positive scalars in the rules affect the rates of the adaptation, but not the direction. Thus the rules above can be simplified:

$$\dot{e}_2 \propto \dot{e}_1\dot{x}_2 \tag{3.45}$$

$$\dot{e}_3 \propto \dot{e}_1(x_2 - D) \tag{3.46}$$

We estimate the reciprocal quality factor by integrating the product of the output error derivative and model output derivative and estimate the reciprocal time constant by integrating the product of the output error derivative and model output without bias.

3.3 Circuit Implementation

3.3.1 Implementation of Log Domain Second Order Filters

We implement the log domain bandpass filter using dynamic MITE networks. The circuit in Figure 3.11(a) is used for the unknown plant and Figure 3.11(b) is used for the estimated model. In subthreshold operation MITE current is an exponential function of the summed inputs.

$$I_1 = I_0 e^{K(V_1 + V_r)} = I_{in} \tag{3.47}$$

$$I_2 = I_0 e^{K(V_1 + V_2)} \tag{3.48}$$

$$I_3 = I_0 e^{K(V_2+V_3)} \tag{3.49}$$

$$I_4 = I_0 e^{K(V_3+V_4)} = I_\tau \tag{3.50}$$

$$I_5 = I_0 e^{K(V_2+V_5)} = I_\tau \tag{3.51}$$

$$I_6 = I_0 e^{K(V_5+V_r)} \tag{3.52}$$

$$I_7 = I_0 e^{K(V_4+V_5)} \tag{3.53}$$

$$I_8 = I_0 e^{K(V_4+V_6)} \tag{3.54}$$

$$I_9 = I_0 e^{K(V_6+V_r)} = I_{DC} \tag{3.55}$$

Kirchoff's Current Law (KCL) is applied at the capacitive nodes to obtain the following relationships:

$$I_\tau / Q + I_3 = I_2 + C\dot{V}_2 \tag{3.56}$$

$$I_8 = I_7 + C\dot{V}_4 \tag{3.57}$$

M6, M7, M8 and M9 form a translinear loop:

$$I_8 = I_7 I_{DC} / I_{64} \tag{3.58}$$

$$I_7 = I_7 I_{DC} / I_6 - C\dot{V}_4 \tag{3.59}$$

M3, M4, M7 and M5 form a translinear loop:

$$I_3 = I_\tau^2 / I_7 \tag{3.60}$$

M1, M2, M5 and M6 form a translinear loop:

$$I_2 = I_{in} I_\tau / I_6 = I_\tau / Q + I_3 - C\dot{V}_2 = I_\tau / Q + I_\tau^2 / I_7 + C\dot{I}_6 / KI_6 \tag{3.61}$$

So the input current can be expressed as

$$I_{in} = I_6 / Q + I_\tau I_6 / I_7 + C\dot{I}_6 / KI_\tau \tag{3.62}$$

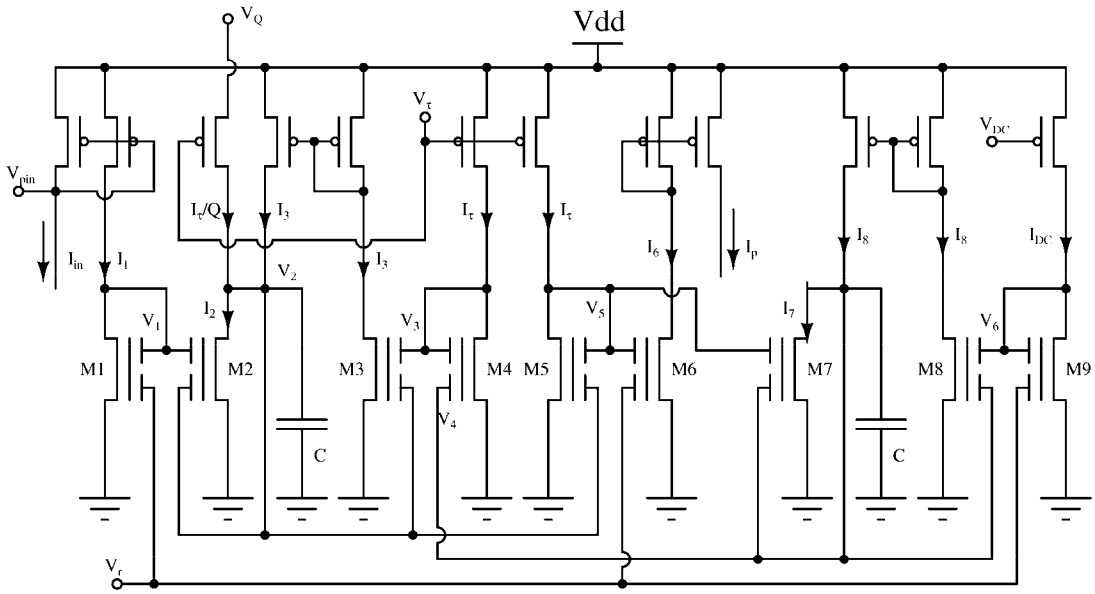

(a)

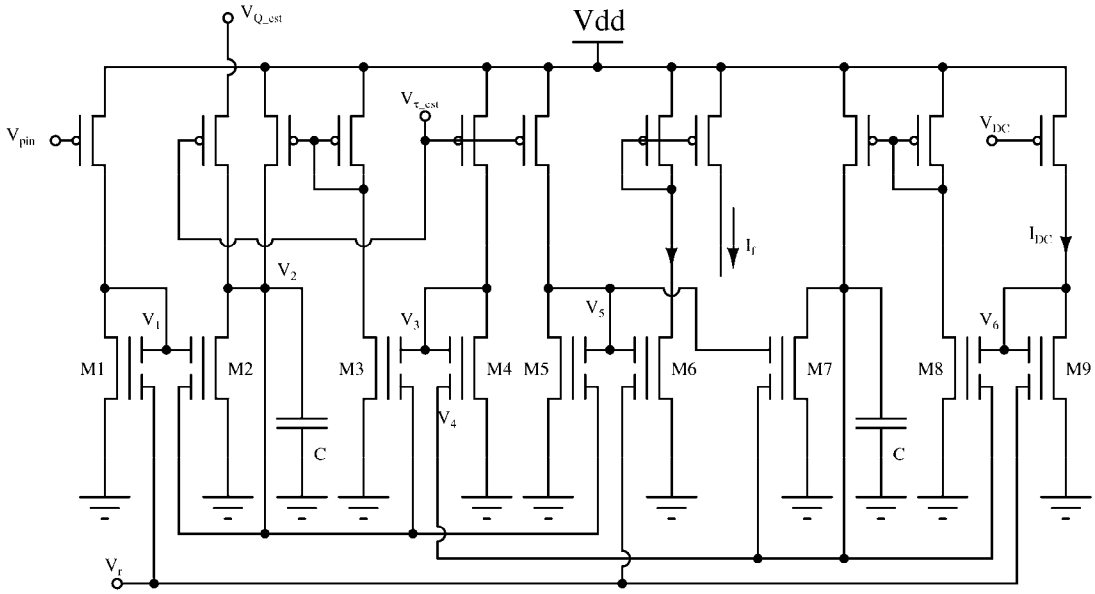

(b)

Figure 3.11: (a) Log domain MITE network for a second order filter used for plant; (b) Log domain MITE implementation for filter.

Let us consider an intermediate current I_x:

$$I_x = I_\tau I_6 / I_7 = I_\tau e^{K(V_r - V_4)} \tag{3.63}$$

$$\dot{I}_x = -I_x K \dot{V}_4 \tag{3.64}$$

$$I_\tau / I_x = I_7 / I_6 \tag{3.65}$$

If we substitute equation (3.59) for I_7,

$$I_\tau I_6 = I_x \left(I_7 I_{DC} / I_6 - C\dot{V}_4 \right) = I_x \left(I_\tau I_{DC} / I_x + C\dot{I}_x / KI_x \right) \tag{3.66}$$

$$C\dot{I}_x / K = I_\tau \left(I_6 - I_{DC} \right) \tag{3.67}$$

$$I_x = KI_\tau \left(I_6 - I_{DC} \right) / sC \tag{3.68}$$

and further substitute the new expression for I_x into equation (3.62), we obtain

$$\begin{aligned} I_{in} &= I_6 / Q + KI_\tau \left(I_6 - I_{DC} \right) / sC + sCI_6 / KI_\tau \\ \Rightarrow I_6 &= \frac{I_{in}\left(sC / KI_\tau \right) + I_{DC}}{1 + \left(sC / KI_\tau \right) / Q + \left(sC / KI_\tau \right)^2} \end{aligned} \tag{3.69}$$

which is a second order transfer function with quality factor Q and time constant $\tau = C/KI_\tau$. We can easily tune the bias current I_τ and bias voltage V_Q to change the time constant and quality factor respectively, thus changing the central frequency and shape of the filter.

3.3.2 Implementation of Learning Rules

The behavior of plant and model filters is controlled by two parameters: quality factor and time constant. We have derived learning rules for the reciprocals of these parameters in section 3.2. The inputs to the learning rules are the temporal derivative of the output difference, the temporal derivative of the model output and the model output excluding bias. Figure 3.12(b) and Figure 3.12(c) are circuits for computing temporal

derivative. We use the circuit of Figure 3.12(b) to implement the derivative of the model output and the circuit of Figure 3.12(c) to implement the derivative of the current output difference.

The structure of the derivative circuit is simply a wide range OTA that operates as a voltage follower with a capacitor connected to the output as shown in Figure 3.12(a). The output current is I_d=I_{d3}-I_{d4} in Figure 3.12(b). The larger the gain, the more accurate the calculation. So we operate the input devices near threshold to maximize transconductance. We use the circuit of Figure 3.12(c) to compute the filter output error e_1 and convert it to a voltage, then realize the derivative $I_{d1} - I_{d2} \propto \dot{e}_1$. The function of V_{bias} in Figure 3.12(c) is to ensure that the input voltage of the derivative circuit remains at an common mode voltage for the differential pair. We also use the intermediate node voltage V_5 of the model filter in Figure 3.11(b) as the input in Figure 3.12(b) in order to compute $I_{d3} - I_{d4} \propto \dot{x}_2$, since $\dot{I}_f = I_f K \dot{V}_5$ and I_f is a positive current which only affects the rate of adaptation. Note that we use a different voltage source V_{cc} for the derivative circuit because the voltage source V_{dd} for the filter circuits in Figure 3.11 is only 1.5V, which is not high enough for the transistors in the derivative circuit to operate in the saturation region.

Both the learning rules for quality factor and time constant require a four quadrant multiplication, and as implemented using the MITE circuits shown in Figure 3.13(a). Circuits for the integrating the learning rules are shown in Figure 3.13(b) and (c), note that V_Q can be higher than V_{dd}, so the voltage V_{ee} in Figure 3.13(b) is higher than V_{dd}.

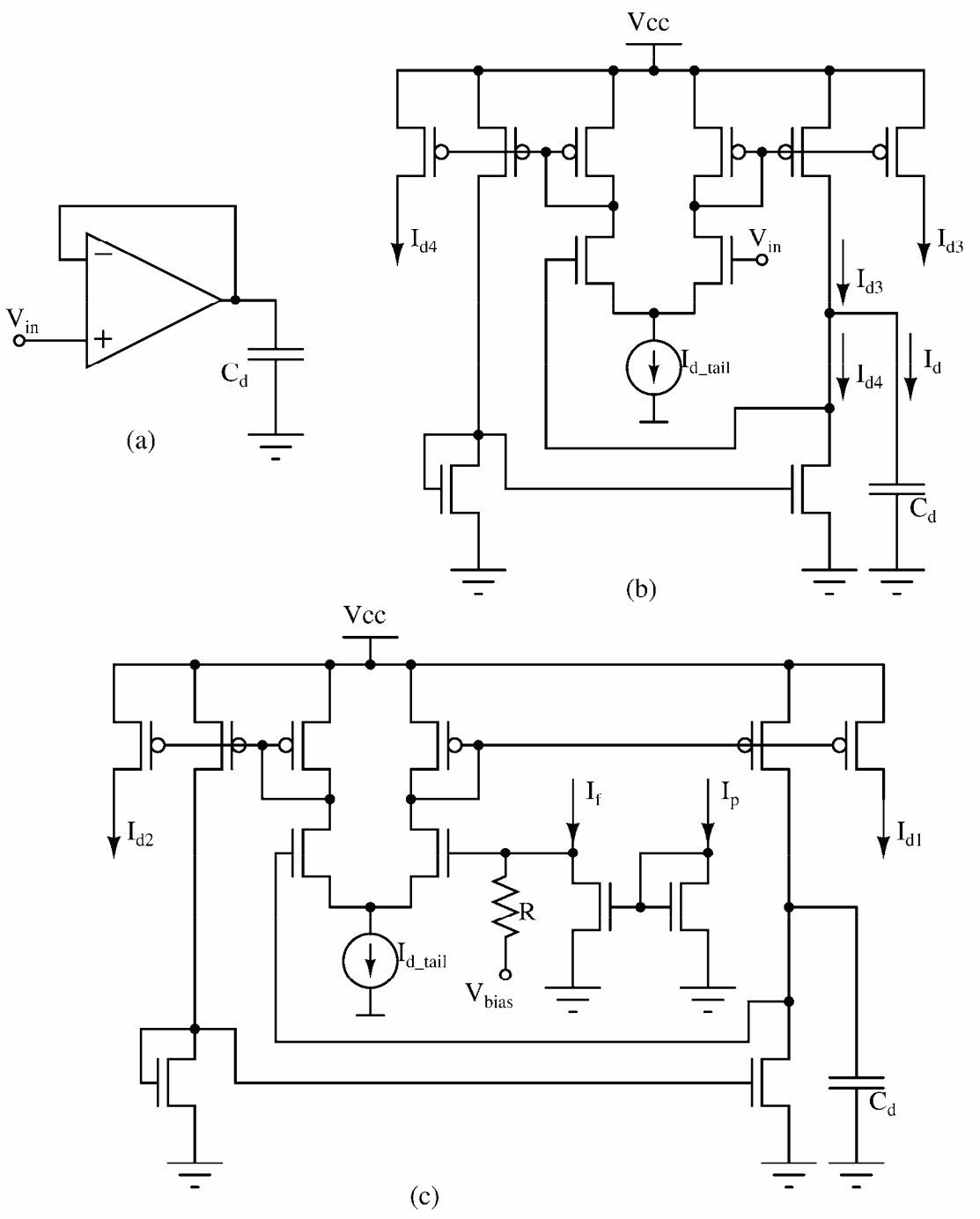

Figure 3.12: (a) and (b) are circuits for computing temporal derivative of voltage; (c) is the circuit for computing temporal derivative of the current output difference.

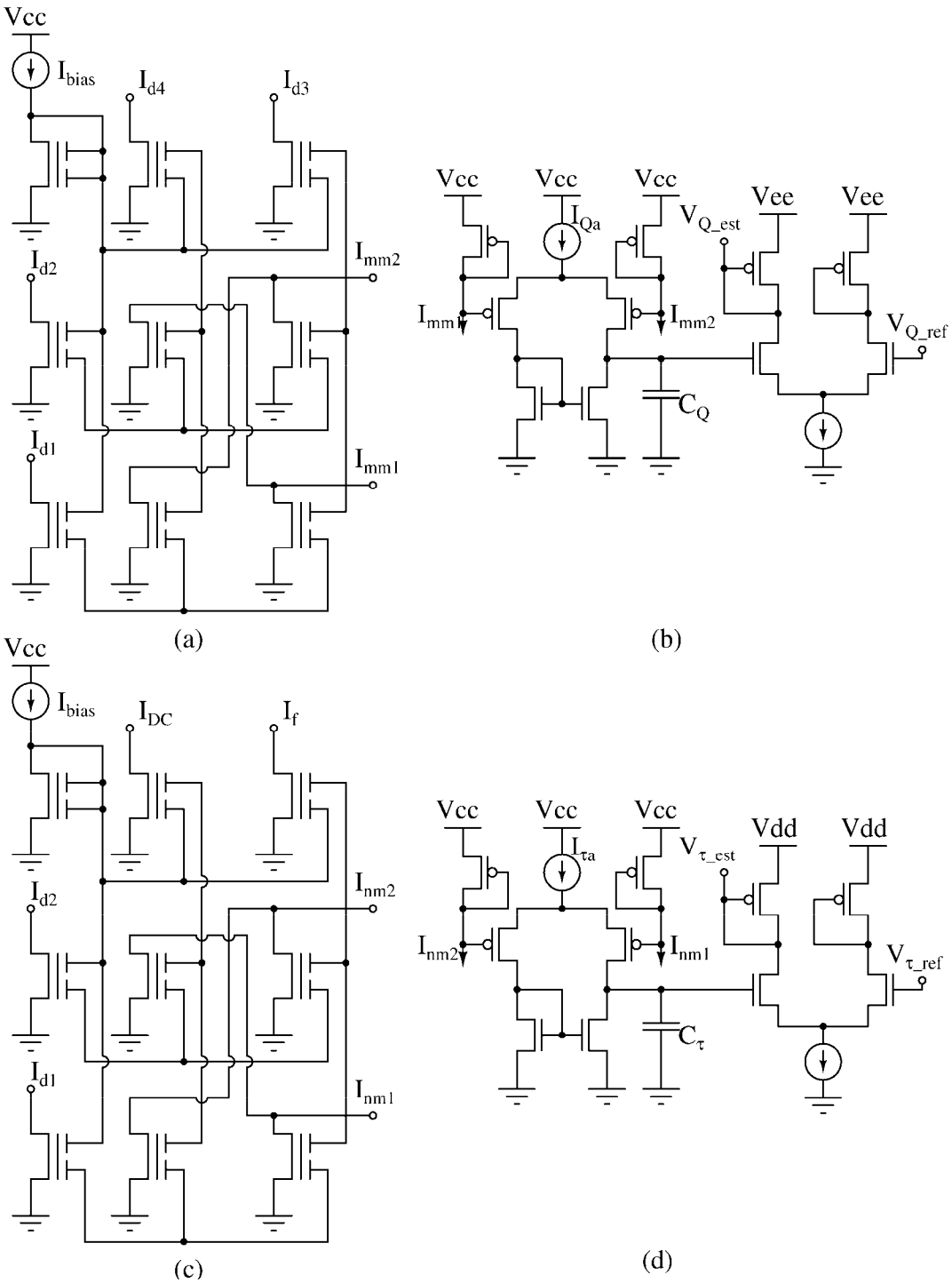

Figure 3.13: (a) Circuit for computing four quadrant multiplication for quality factor adaptation; (b) Integrator circuit for quality factor adaptation; (c) Circuit for computing four quadrant multiplication for time constant adaptation; (d) Integrator circuit for time constant adaptation.

3.4 Simulation Results

The circuit is simulated with HSPICE using BSIM3v3 model for a commercially available 0.5μm technology. The technique in [14] is used to avoid floating-node problems in the simulation. The diagram is shown in Figure 3.14. We add a voltage-dependent voltage source $V_{floating\_gate}$ from ground to the floating gate through a big resistor R. There is no current through R, because $V_{floating\_gate}$ tracks the floating gate voltage itself. This artificial DC path to ground aids numerical convergence in HSPICE simulator. The voltage source V_{dd} for both filters is 1.5V and the voltage sources V_{cc} and V_{ee} required for adaptation are both 2.5V. We use a sine wave (Figure 3.15) and superposition of sine waves (Figure 3.16 and Figure 3.17) as inputs.

Figure 3.15 shows adaptation with a 10kHz sine wave. The sine wave is biased at 100nA with a peak to peak variation of 120nA. Figure 3.15(a) shows V_Q and V_{Q_est}. V_Q is varied as 1.47V from 0-2ms, 1.45V from 2-6ms and 1.46V from 6-10ms. Figure 3.15(b) shows V_τ and V_{τ_est}. The different V_τ values correspond to different values of I_τ. I_τ is varied as 40nA from 0-4ms, 45nA from 4-8ms, and 35nA from 8-10ms. Figure 3.15(c) is the error between the plant and filter output. For all changes in V_Q and V_τ, V_{Q_est} and V_{τ_est} track the new values accurately. The error converges to zero when V_{Q_est} converges to V_Q and V_{τ_est} converges to V_τ. The adaptation rate depends on signal strength, currents I_{Qa} and $I_{\tau a}$, and capacitances C_Q and C_τ.

Next we show adaptation when the input signal is a mixture of sine waves. In Figure 3.16, the input signal is a combination of equally weighted sine waves at 10kHz, 20kHz, 40kHz and 80kHz as input. The DC current is also 100nA and each of the sine waves has

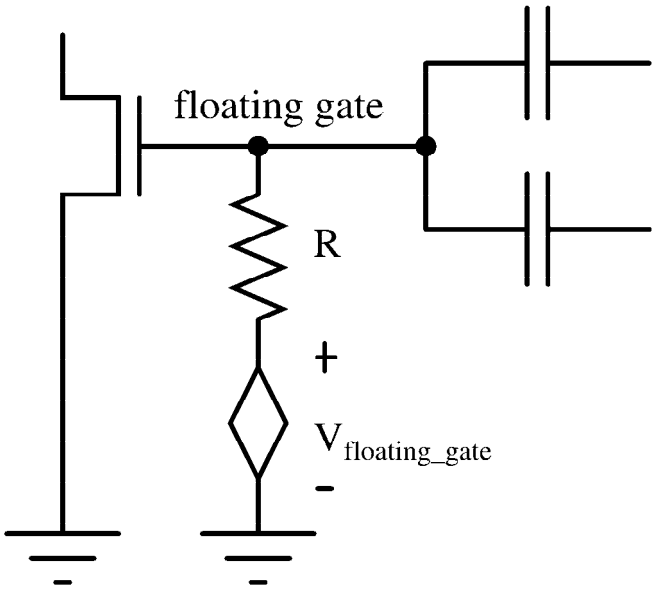

Figure 3.14 Technique used to avoid floating-node problems in the simulator.

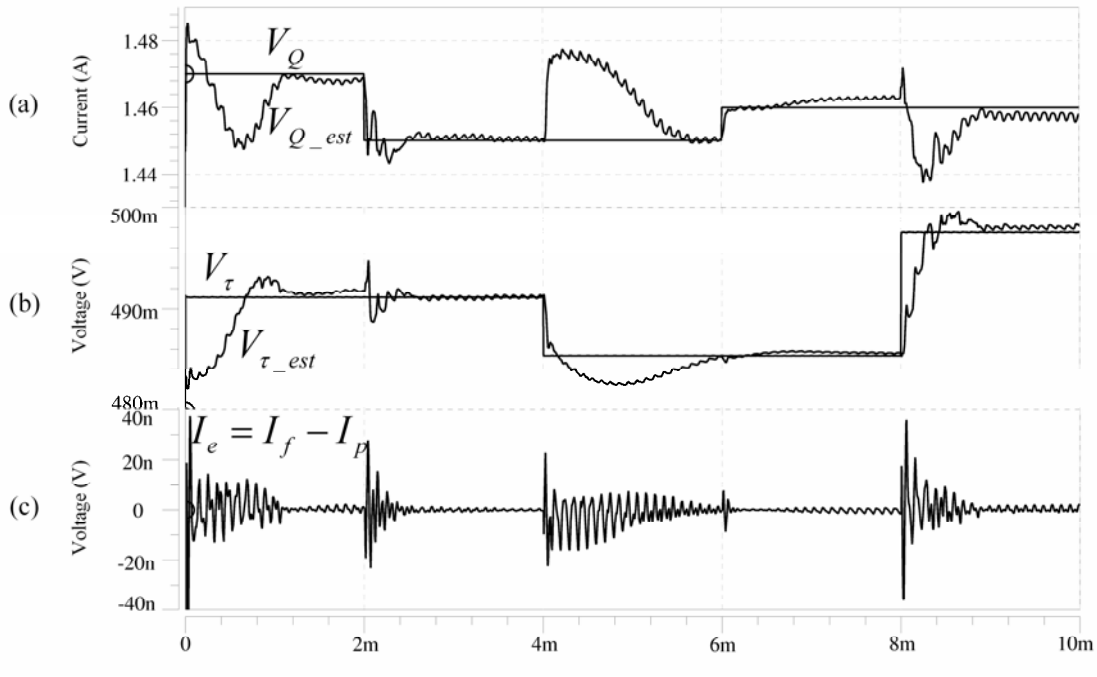

Figure 3.15: 10kHz sine wave input signal: (a) Quality factor adaptation. (b) Time constant adaptation. (c) Output error.

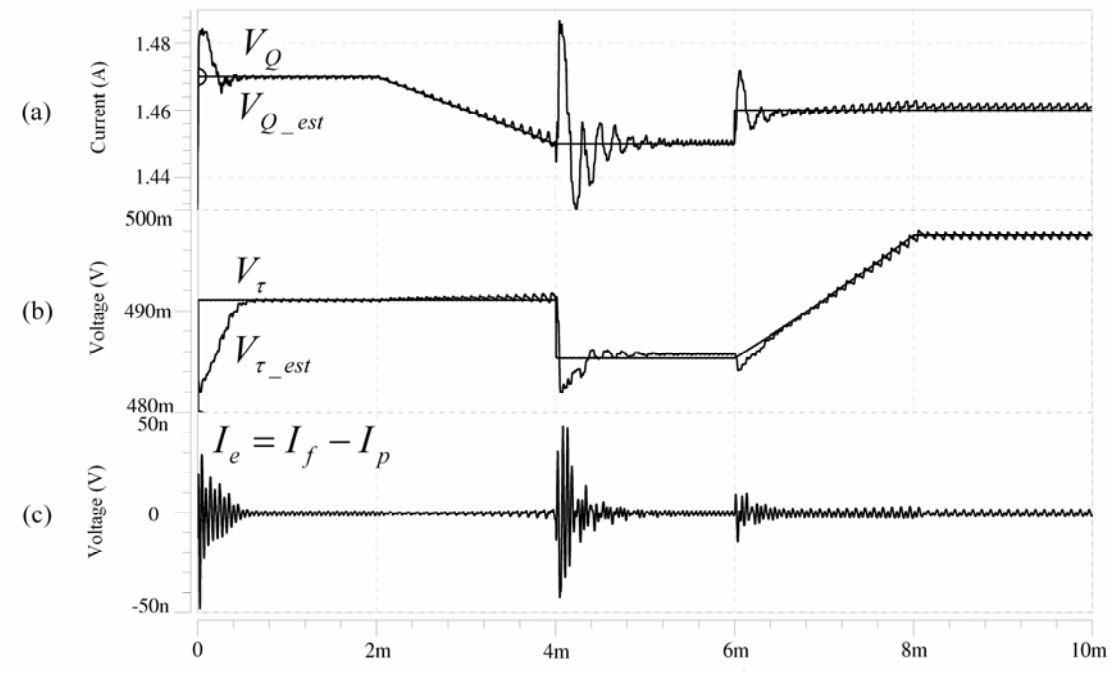

Figure 3.16: Four harmonic sine waves input signal: (a) Quality factor adaptation. (b) Time constant adaptation. (c) Output error.

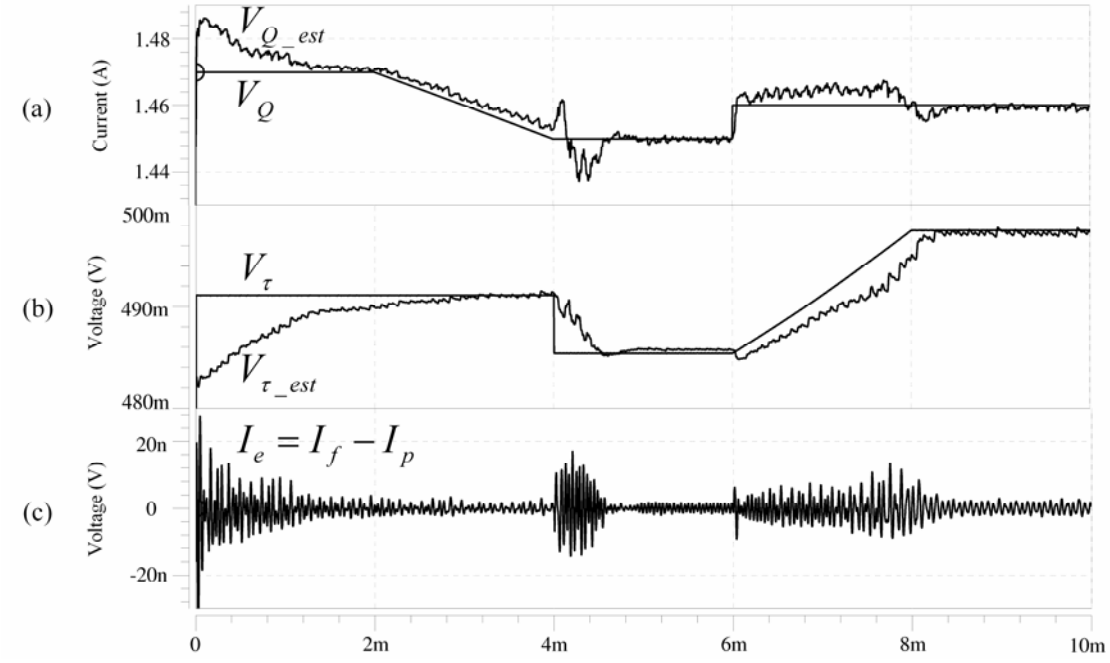

Figure 3.17: Six geometrically spaced sine waves from 10-96kHz input signal: (a) Quality factor adaptation. (b) Time constant adaptation. (c) Output error.

a peak to peak variation of 30nA. In Figure 3.17, the input signal is a summation of 6 equally weighted sine waves, whose frequency ratio is an irrational number $\pi/2$, spanning from 10kHz to 96kHz.The sine wave is also biased at 100nA and each of the sine waves has a peak to peak variation of 20nA. In each case, V_{Q_est} accurately tracks V_Q as shown in Figure 3.16(a) and Figure 3.17(a) and V_{τ_est} tracks V_τ, as shown in Figure 3.16(b) and Figure 3.17(b) and the output error shown in Figure 3.16(c) and Figure 3.17(c) approaches zero when adaptation is finished.

3.5 Summary

A circuit design approach has been developed for log domain adaptive filters that extends earlier work from adaptation of first order lowpass filters to a second order structure. A novel structure has been designed for a second order filter using a log domain topology which has wide tuning range and large dynamic range and capability for high frequency operation. Further, robust learning rules have been developed for system identification based on the direct Lyapunov method for the second order filter. These learning rules have been implemented using MITE structures, which are compact and elegant, although necessarily more complex than the design of the adaptive first order lowpass filter. Simulation results demonstrate the validity of the learning rules. Future work will focus on fabricating these circuits, experimentally validating these results and extending this work to more comprehensive adaptive filter structures.

Chapter 4: Conclusions and Future work

In this thesis, we have developed two circuit design approaches for log domain adaptive filters. One is an adaptive first order lowpass filter, the other is an adaptive second order tunable filter. Both of them utilize log domain filters implemented with MITE circuits to integrate learning rules for system identification. The second order filter is a novel structure using a log domain topology to implement compact current mode IIR filters that operate with low power, have wide tuning range and large dynamic range and capability for high frequency operation. Further, robust learning rules for the parameters of the two adaptive systems are derived based on Lyapunov stability. These learning rules are implemented using MITE structures, highlighting the elegance and symbiotic nature of the design methodology.

Simulation results with HSPICE using BSIM3v3 models are presented for both the first order lowpass filter and the second order bandpass filter with a tunable bias current. The log domain filters adapt to estimate the parameters of the reference filters accurately and efficiently as the parameters are changed. The output difference between the estimated system and the reference system approaches zero when adaptation is complete.

The first order lowpass adaptive filter has been designed and fabricated in a commercially available 0.5μm CMOS technology. Experimental results for the first order lowpass filter show stable adaptation under a variety of conditions, which proves the success of the adaptive system using this model-based learning method. The measured power consumption is only 33μW which justifies low power operation of MITE structures.

Future work will focus on fabricating the circuits of the adaptive second order log domain filters, experimentally validating these results and extending this work to more comprehensive adaptive filter structures.

Bibliography

[1] Hasler, P., Minch, B.A. and Diorio, C., "An Autozeroing Floating-Gate Amplifier," IEEE Transactions on Circuits and Systems II: Analog and Digital Signal Processing, vol. 48, issue 1, pp. 74-82, Jan. 2001.

[2] Fernandez, R., Lopez-Martin, A.J., de la Cruz, C.A., Carlosena, A., "A 1V micropower FGMOS Log-Domain Filter," International Conference on Electrons, Circuits and Systems, vol. 1, pp381-384, 15-18 Sept. 2002.

[3] Rodriguez-Villegas, E., Yufera, A., Rueda, A., "A 1-V micropower log-domain integrator based on FGMOS transistors operating in weak inversion," IEEE Journal of Solid-State Circuits, vol. 39, issue 1, pp.256-259, Jan. 2004.

[4] Minch, B.A., Hasler, P. and Diorio, C., "Multiple-Input Translinear Element Networks," IEEE Transactions on Circuits and Systems II, vol. 48, issue 1, pp. 20-28, Jan. 2001.

[5] Minch, B.A., "Multiple-Input Translinear Element Log-Domain Filters," IEEE Transactions on Circuits and Systems II: Analog and Digital Signal Processing, vol. 48, issue 1, pp. 29-36, Jan. 2001.

[6] Minch, B.A., "Synthesis of Static and Dynamic Multiple-Input Translinear Element Networks," IEEE Transactions on Circuits and Systems I, vol. 51, issue 2, pp.409-421, Feb. 2004.

[7] El-Masry, E.I., Gates, J.W., "A Novel Continuous-Time Current-Mode Differentiators and Its Applications," IEEE Transactions on Circuit and Systems II, vol.43, No. 1, Jan 1996

[8] Wu, J., and El-Masry, E., "Current-mode ladders filters using multiple output current conveyors," IEEE Proceedings on Circuits, Devices and Systems, vol.143, Issue,4, pp.218-222, Aug 1996

[9] Juan, J.-K., Harris, J.G. and Principe, J.C., "Analog Hardware Implementation of Adaptive Filter Structures," International Conference on Neural Networks, vol. 2, pp. 916-921, 9-12 June 1997.

[10] Stanacevic, M. and Cauwenberghs, G., "Charge-Based CMOS FIR Adaptive Filter," Proceedings of the 43rd IEEE Midwest Symposium on Circuits and Systems, vol.3, pp. 1410-1413, 8-11 Aug. 2000.

[11] Ferrara, E.R. Jr., Widrow B., "The Time-Sequenced Adaptive Filter", IEEE Transactions on Circuit and Systems, vol. cas-28, No. 6, June 1981

[12] Abshire, P.A., Wong, E.L., Zhai, Y. and Cohen, M., "Adaptive Log Domain Filters Using Floating Gate Transistors," Proceedings of the 2004 International Symposium on Circuits and Systems, vol. 1 , page I-29 - I-32, 23-26 May 2004.

[13] Narendra, K.S. and Anaswamy, A.M., *Stable Adaptive Systems*, Prentice-Hall, New Jersey, 1989

[14] Rahimi, K., Diorio, C., Hernandez, C., Brockhausen, M.D., "A Simulation Model for Floating-Gate MOS Synapse Transistors, " IEEE International Symposium on Circuits and Systems, vol.2, pp. II-532 - II-535, 26-29 May 2002.

[15] Horowitz, P. and Hill, W. *The Art of Electronics,* Cambridge University Press, Cambridge, 1989

[16] Zhai, Y. and Abshire, P.A., "A 1.5V Low Power Second Order Bandpass Filter Using Floating Gate Transistors, " submitted for IEEE International Symposium on Circuits and Systems, 2005.

[17] Zhai, Y. and Abshire, P.A., "Adaptation of Log Domain Second Order Filters Implemented by Floating Gate MOSFETs, " submitted for IEEE International Symposium on Circuits and Systems, 2005.

[18] Edwards, T.R., "Time-Frequency Acoustic Processing and Recognition: Analysis and Analog VLSI Implementations, " Chapter 3, PhD dissertation, Department of Computer and Electrical Engineering, John Hopkins University, 1999.